

UCLA

UCLA Previously Published Works

Title

Crystal nucleation and growth of spherulites demonstrated by coral skeletons and phase-field simulations

Permalink

<https://escholarship.org/uc/item/26g501w7>

Authors

Sun, Chang-Yu

Gránásy, László

Stifler, Cayla A

et al.

Publication Date

2021

DOI

10.1016/j.actbio.2020.06.027

Peer reviewed

Manuscript Number: AB-20-1031R2

Title: Crystal nucleation and growth of spherulites demonstrated by coral skeletons and phase-field simulations

Article Type: SI: BIOMIN 19

Keywords: Crystal nucleation, crystal growth, coral, spherulite, sprinkle, polymer, semicrystalline. Stylophora pistillata, Balanophyllia, Oculina, Phyllangia, Turbinaria, Acropora, Madracis, Porites, Favia, Blastomussa, Montipora, Micromussa.

Corresponding Author: Professor Pupa U. P. A. Gilbert, Ph.D.

Corresponding Author's Institution: University of Wisconsin - Madison

First Author: Pupa U. P. A. Gilbert, Ph.D.

Order of Authors: Pupa U. P. A. Gilbert, Ph.D.; Chang-Yu Sun, BS

Abstract: Spherulites are radial distributions of acicular crystals, common in biogenic, geologic, and synthetic systems, yet exactly how spherulitic crystals nucleate and grow is still poorly understood. To investigate these processes in more detail, as a model system we chose corals, which are well known to form their skeletons from aragonite (CaCO₃) spherulites, and because a comparative study of crystal structures across coral species has not been performed previously. We observed that all 12 diverse coral species analyzed here exhibit plumose spherulites in their skeletons, with well-defined centers of calcification (CoCs), and crystalline fibers radiating from them. In 7 of the 12 species, we observed a skeletal structural motif not observed previously: randomly oriented, equant crystals, which we termed "sprinkles". In *Acropora pharaonis*, these sprinkles are localized at the CoCs, while in 6 other species sprinkles are either layered at the growth front (GF) of the spherulites, or randomly distributed. At the micro-scale, coral skeletons fill space as much as single crystals of aragonite. Based on these observations, we tentatively propose a spherulite formation mechanism in which growth front nucleation (GFN) of randomly oriented sprinkles, competition for space, and coarsening (either by Ostwald or Smoluchowski ripening) produce spherulites, rather than the previously assumed slightly misoriented nucleations termed "non-crystallographic branching". Phase-field simulations support this mechanism, and, using a minimal set of thermodynamic parameters, are able to reproduce all of the microstructural variation observed experimentally in all of the investigated coral skeletons. Beyond coral skeletons, other spherulitic systems, from aspirin to semicrystalline polymers and chocolate, may also form according to the mechanism for spherulite formation proposed here.

Statement of Significance.

Understanding the fundamental mechanisms of spherulite nucleation and growth has broad ranging applications in the fields of metallurgy, food science, and pharmaceutical production. Using the skeletons of reef-building corals as a model system for investigating these processes, we propose a new spherulite growth mechanism that can not only explain the micro-structural diversity observed in distantly related coral species, but may point to a universal growth mechanism in a wide range of biologically and technologically relevant spherulitic materials systems.

Response to Reviewers for AB-20-1031R1

Our responses are in blue font, and the comments from the editor and the reviewers are in black font, and reproduced below in their entirety. The changes in the manuscript are highlighted in cyan.

Comments:

Editor: Your manuscript is almost ready for acceptance. Prior to that, may I ask you to consider the comment of reviewer 2 and the following editorial requests?

Thank you! We are glad to comply.

1) Please submit the figure captions separately without the figures;

Done. The figures are now removed from the Figure Captions file. The tables and captions remain in this file.

2) Please try to develop your graphical abstract to be more than just one image. For more information and examples of good graphical abstracts consult the author guideline:

<https://www.elsevier.com/authors/journal-authors/graphical-abstract>;

Done.

3) Please specifically try to remove words such as "novel" and "new" and use a more explicit and scientific terminology. We expect authors to present "novel" results / approaches / techniques, so the use of "new" and "novel" are not necessary;

We removed all instances of "new" and "novel" for results or mechanisms, but kept all cases in which "new" referred to a nucleation event during the mechanism.

See pages 2, 15, 21.

4) Please consider editing the title to the following or similar: "Crystal nucleation and growth in spherulites as demonstrated by the evaluation of coral skeletons".

Done. We changed it to "Crystal nucleation and growth of spherulites demonstrated by coral skeletons and phase-field simulations"

Reviewer #2: This is an example of the growth of biomimetic films.

<https://onlinelibrary.wiley.com/doi/abs/10.1002/adfm.201202294>

We thank the reviewer for pointing out this magnificent paper. We have cited it and completely agree with the reviewer that there are beautiful similarities between the in-vitro 2D system and the coral 3D system! We cite the paper as ref 95 on page 15, and more extensively on page 20:

"In mesocrystalline polymer films, sprinkles are occasionally observed, interspersed with

acicular spherulitic crystals (see figure 2B in ref. [95]). The acicular crystals grow and surround sprinkles, exactly as they do in coral skeletons (e.g. Fig. 2b arrows).”

In Figure 1 d-e, Figure 2a-c, and Figure 4a-d, the authors can find that the growth of each single crystalline domain is independent and irreversible. They stop growing when adjacent domains get in touch with each other. We should point out that we cannot exclude the possibility that dissolution-recrystallization can happen in coral, as assumed in the paper. But according to our experience, we were never able to collect data supporting the dissolution-recrystallization pathway in the course of mineralization of biomimetic films.

We completely agree that coarsening, either by dissolution-precipitation, or by a solid-state transformation (termed Ostwald and Smoluchowski ripening, respectively) were not observed before in other spherulitic systems. We provided strong evidence in this paper, thus the lack of previous observation does not subtract, it adds to the significance of this manuscript. We stress that nucleation of randomly oriented sprinkles and their coarsening occurs in all spherulites, including the ones in ref. 95 by Jiang et al. 2013. It just happens at the nanoscale, whereas the authors document beautifully the behavior of PILP droplets, spherulites, and final crystals with (polarized) optical microscopy at the microscale. If they wish, they could look at the same quaternary polymer system frozen in time, using TEM to observe sprinkles at the nanoscale.

This issue was also raised by Review 3 ("Additionally, the growth model is interesting, but I have problems to understand that previously formed sprinkles may disappear by dissolution, solid-state transformation or any other of the processes invoked. It is never proven that this happens in coral skeletons.").

We have previously explained to Reviewer #3 that coarsening may happen by Ostwald or Smoluchowski ripening, and these are both well-known phenomena. We know it's hard to imagine them for all of us in biomineralization, but they are well established in the materials community.

We kindly ask the authors to rethink of the scenario of coral growth.

We don't think a complete overhaul of the key concept in this paper is needed at this late stage in the peer-reviewing process. Especially not on the basis that in a *different* system and at a *different* scale the authors of Jiang et al. 2013 did not observe coarsening.

Reviewer #3: I acknowledge the in-depth review carried out by the authors. In fact, almost all my concerns about the contents of the manuscript have now subsided. The few which have not (the true nature of sprinkles in some of the illustrations, the effect of the

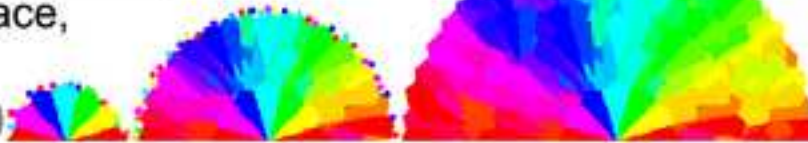
calcifying fluid in sprinkle dissolution) are very minor and I have to recognize that they are open questions. Additionally, they do not affect the essence of the study.

Thank you for your careful re-reading of the paper, and your kind remarks. We look forward to the answers to all of the open questions, which will be provided by other groups and ours, in a variety of other systems organic, mineral, or biomineral.

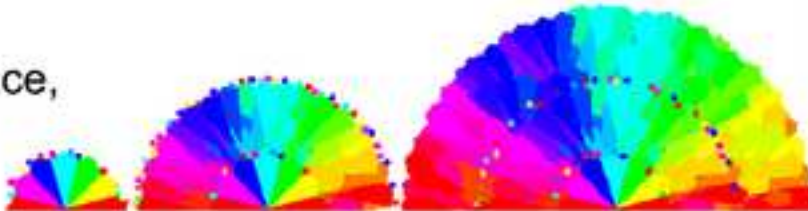
For further assistance, please visit our customer support site at <http://help.elsevier.com/app/answers/list/p/7923>. Here you can search for solutions on a range of topics, find answers to frequently asked questions and learn more about EES via interactive tutorials. You will also find our 24/7 support contact details should you need any further assistance from one of our customer support representatives.

spherulites

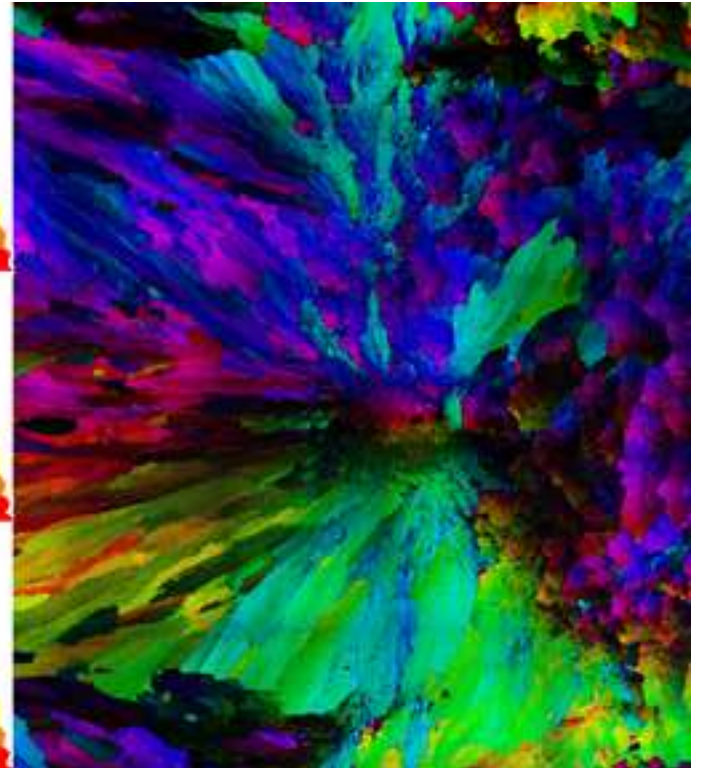
randomly-oriented nucleations,
competition for space,
coarsening
(all spherulites)



competition for space,
no coarsening
(few corals)



non-crystallographic
branching
(never)



1
2
3
4
5
6
7
8
9
10
11
12
13
14
15
16
17
18
19
20
21
22
23
24
25
26
27
28
29
30
31
32
33
34
35
36
37
38
39
40
41
42
43
44
45
46
47
48
49
50
51
52
53
54
55
56
57
58
59
60
61
62
63
64
65

Crystal nucleation and growth of spherulites demonstrated by coral skeletons and phase-field simulations

Chang-Yu Sun^{1,2}, László Gránásy³, Cayla A. Stifler¹, Tal Zaquin⁴, Rajesh V. Chopdekar⁵,
Nobumichi Tamura⁵, James C. Weaver⁶, Jun A. Y. Zhang¹, Stefano Goffredo⁷, Giuseppe Falini⁸,
Matthew A. Marcus⁵, Tamás Pusztai³, Vanessa Schoeppler⁹, Tali Mass⁴, Pupa U. P. A.
Gilbert^{1,10, §,*}

¹ Department of Physics, University of Wisconsin, Madison, WI 53706, USA

² Materials Science Program, University of Wisconsin, Madison, WI 53706, USA

³ Institute for Solid State Physics and Optics, Wigner Research Centre for Physics, PO Box 49,
1525 Budapest, Hungary.

⁴ University of Haifa, Marine Biology Department, Mt. Carmel, Haifa 31905, Israel.

⁵ Advanced Light Source, Lawrence Berkeley National Laboratory, Berkeley, CA 94720, USA.

⁶ Wyss Institute for Biologically Inspired Engineering, Harvard University, Cambridge, MA 02138,
USA.

⁷ Marine Science Group, Department of Biological, Geological and Environmental Sciences,
University of Bologna, Via Selmi 3, I-40126 Bologna, Italy.

⁸ Department of Chemistry “Giacomo Ciamician”, Alma Mater Studiorum – University of
Bologna, Via Selmi 2, 40126 Bologna, Italy.

⁹ B CUBE–Center for Molecular Bioengineering, Technische Universität Dresden, 01307
Dresden, Germany.

¹⁰ Departments of Chemistry, Geoscience, Materials Science, University of Wisconsin, Madison,
WI 53706, USA.

1
2
3
4 § previously publishing as Gelsomina De Stasio

5
6 * Correspondence to: pupa@physics.wisc.edu

7
8 **ABSTRACT:** Spherulites are radial distributions of acicular crystals, common in biogenic,
9 geologic, and synthetic systems, yet exactly how spherulitic crystals nucleate and grow is still
10 poorly understood. To investigate these processes in more detail, as a model system we chose
11 corals, which are well known to form their skeletons from aragonite (CaCO₃) spherulites, and
12 because a comparative study of crystal structures across coral species has not been performed
13 previously. We observed that all 12 diverse coral species analyzed here exhibit plumose
14 spherulites in their skeletons, with well-defined centers of calcification (CoCs), and crystalline
15 fibers radiating from them. In 7 of the 12 species, we observed a skeletal structural motif **not**
16 **observed previously:** randomly oriented, equant crystals, which we termed “sprinkles”. In
17 *Acropora pharaonis*, these sprinkles are localized at the CoCs, while in 6 other species
18 sprinkles are either layered at the growth front (GF) of the spherulites, or randomly distributed.
19 At the micro-scale, coral skeletons fill space as much as single crystals of aragonite. Based on
20 these observations, we tentatively propose **a spherulite formation mechanism** in which growth
21 front nucleation (GFN) of randomly oriented sprinkles, competition for space, and coarsening
22 (either by Ostwald or Smoluchowski ripening) produce spherulites, rather than the previously
23 assumed slightly misoriented nucleations termed “non-crystallographic branching”. Phase-field
24 simulations support this mechanism, and, using a minimal set of thermodynamic parameters,
25 are able to reproduce all of the microstructural variation observed experimentally in all of the
26 investigated coral skeletons. Beyond coral skeletons, other spherulitic systems, from aspirin to
27 semicrystalline polymers and chocolate, may also form according to the mechanism for
28 spherulite formation **proposed here**.

29
30
31
32
33
34
35
36
37
38
39
40
41
42
43
44
45
46
47
48
49
50
51
52
53
54
55 **Keywords.**

1
2
3
4 Crystal nucleation, crystal growth, coral, spherulite, sprinkle, polymer, semicrystalline.
5
6 *Stylophora*, *Balanophyllia*, *Oculina*, *Phyllangia*, *Turbinaria*, *Acropora*, *Madracis*, *Porites*, *Favia*,
7
8 *Blastomussa*, *Montipora*, *Micromussa*.
9

10 11 12 **1. Introduction.** 13

14
15
16 Spherulites comprise acicular crystals radiating from common centers. They are widespread
17
18 and can be formed in metals [1], polymers or organic molecules [2-5], minerals crystallizing from
19
20 melts [6, 7], and biominerals, including eggshells [8], otoliths [9], kidney stones [10], and coral
21
22 skeletons [11, 12]. While it is well known that spherulites grow into spheres at micron, millimeter,
23
24 or even centimeter scales [5, 13], the nucleation and growth mechanisms at the nanometer
25
26 scale are poorly understood. Early studies from the late 1800s and early 1900s recognized that
27
28 spherulitic structures analogous to those observed geologically were observed in coral
29
30 skeletons [14, 15], but were suggested to be simply physicochemical results of “competition for
31
32 space” during crystal growth [16]. Other studies investigating coral skeletal formation, revealed
33
34 that organics, including proteins [17, 18] and polysaccharides [19, 20], play important roles in
35
36 the nucleation, polymorph selection [21], crystal morphology, and orientation [22, 23]. Exactly
37
38 how crystals form spherulites in coral skeletons thus remains unsettled.
39
40
41

42
43 In order to gain insight into the fundamental formation mechanism of spherulitic crystal growth,
44
45 in the present study we analyzed the skeletons of a wide range of morphologically diverse, and
46
47 distantly related scleractinian corals, also known as stony corals, because they form hard
48
49 aragonite (CaCO₃) skeletons.
50

51
52 At the centimeter scale, the skeletons of scleractinian corals are morphologically diverse: they
53
54 can be massive as in *Favia* sp. and *Porites* sp., branching as in *Stylophora* sp. and *Acropora*
55
56 sp., encrusting as in *Phyllangia* sp. and *Oculina* sp., or table-like as in *Turbinaria* sp. At the
57
58 microscopic scale, however, all modern stony coral skeletons reveal morphological similarities,
59
60

1
2
3
4 displaying needle-like aragonite crystal fibers radiating from centers of calcification (CoCs) [16,
5
6 24-32], and forming plumose spherulites [11, 22, 33-36].
7

8
9 Historically, spherulites have been defined as a radial distribution of acicular crystals with a
10
11 common center point, forming a spherical geometry. The center, however, does not have to be a
12
13 single point; it can be a straight or curved line, or even a two-dimensional surface.
14

15
16 If the centers are along lines or surfaces, spherulites are termed “plumose”, as their cross-
17
18 sections resemble plumes or feathers. Despite their name, in three-dimensions, plumose
19
20 spherulites resemble bottle brushes or feather dusters, more than single, two-dimensional
21
22 feathers. In coral skeletons, the spherulites observed here and previously are plumose
23
24 spherulites.
25

26
27 A variety of methods have been used to characterize coral spherulites, all demonstrating that
28
29 CoCs have a micro-granular structure [37-39], and in contrast to their adjacent aragonitic fibers,
30
31 contain both aragonite and a stable amorphous calcium carbonate, and greater concentrations
32
33 of magnesium and organics [19, 40-45].
34

35
36 Although all previous studies of coral skeletal fibers observed and described the radial
37
38 distribution of their crystal long axes, there are, thus far, only two reports (from *Porites* sp. and
39
40 *Stylophora pistillata* [11, 12]) describing, quantitatively, their precise crystal orientation directions
41
42 and thus confirming unambiguously that coral skeleton growth in these two species is indeed
43
44 spherulitic. Due to this limited sample size, however, several questions regarding the details of
45
46 coral skeleton formation remain:
47

- 48 a. Do other corals also form their skeletons spherulitically or are there alternative growth
49
50 modes?
51
- 52 b. Are the *c*-axes of aragonite crystal fibers oriented along the radial growth direction?
53
- 54 c. How do spherulites grow? Can we learn new insights from the study of a diverse set of
55
56 coral skeletons regarding how spherulitic growth occurs?
57
58

1
2
3
4 d. If so, can the insights be generalized beyond coral skeletons to other materials systems?
5

6 The answers to the first two questions above are not as trivial as they might appear, based
7 exclusively on the morphology of coral skeletons. To illustrate this point in a different biomineral
8 system, in human enamel it was long established that nanocrystals in each enamel rod are
9 elongated, parallel to one another, and co-oriented. Recent analysis, however, demonstrated
10 that those morphologically parallel crystals are not at all co-oriented, nor is the *c*-axis of each
11 nanocrystal oriented along the crystal's long axis [46]. To a much smaller extent, this effect was
12 also observed in parrotfish teeth [47]. In contrast, in synthetic hydroxyapatite spherulites, and
13 synthetic [11] and biogenic aragonite spherulites [48], the *c*-axes are oriented along each
14 crystal's long axis [49]. Together, these results obtained from different crystal systems
15 demonstrate that crystal long axes and *c*-axes are not necessarily parallel.
16
17
18
19
20
21
22
23
24
25
26
27

28 To avoid confusion, and from this point forward, crystallites of any kind will be called "grains" to
29 conform with the common materials science terminology. In coral skeletons, these grains are
30 the micro- or nano-crystals usually termed fibers or CoCs by coral researchers.
31
32

33 Much of the confusion regarding the spherulitic growth of coral skeletons stems from the
34 observation that the outer surface, which is the growth front of a coral skeleton, may or may not
35 be spherulitic in morphology [20, 50, 51]. For example, Figure 1 shows scanning electron
36 microscopy (SEM) images of corallites from three distantly related coral genera (Fig. S1).
37
38
39

40 Despite the fact that the bulk, mature skeletons exhibit a distinctly spherulitic morphology, the
41 growth fronts may vary from the smooth and disordered *Cyphastrea* sp. to the well-defined
42 particle-like crystallites of *Balanophyllia* sp. (Fig. 1). Previous studies on the ultrastructure of
43 sectioned coral skeletons using SEM and TEM [12, 48, 52], Polarized Light Microscopy (PLM)
44 [22, 36], and Electron Back Scatter Diffraction (EBSD) [53, 54], however, have only revealed the
45 presence of spherulitic aragonite, with no indication of the presence of these smaller-scale
46 particulate features. Thus, the goals of the present study (questions a. and b.) are to investigate
47
48
49
50
51
52
53
54
55
56
57
58
59

1
2
3
4 the potentially widespread nature of this particle-like skeletal structural motif, identify key
5 skeletal maturation pathways (questions c. and d.), and attempt to reconcile the particles at the
6 skeleton growth front described here (Fig. 1) with those reported previously [20, 51, 55, 56] and
7 their proposed formation mechanism. To address these questions, we present here 60-nm
8 resolution, large area (up to $200 \times 300 \mu\text{m}^2$), crystal orientation maps acquired with Polarization-
9 dependent Imaging Contrast (PIC) mapping, which uses PhotoEmission Electron
10 spectroMicroscopy (PEEM) [11, 57-61], from the skeletons of 12 distantly related and
11 morphologically diverse coral species. The results obtained from these structural
12 characterization studies will also be used to validate contrasting hypotheses related to growth
13 front nucleation (GFN), an umbrella term that includes all possible microscopic mechanisms that
14 lead to the formation of grains of new orientations at the growth front [62]. Historically,
15 nucleation of crystals with slight misorientation has been called “non-crystallographic branching”
16 (NCB), and has been assumed to explain how spherulitic crystals nucleate and grow [3, 4, 63,
17 64]. These mechanisms, however, still need experimental verification, and this paper is aimed at
18 addressing precisely this point using coral skeletons as a model system.

2. Materials and Methods.

39 Detailed materials and methods are provided in Appendix A. Briefly, coral skeletons (A.1) were
40 embedded, polished, coated as described previously [65], and imaged on the PEEM-3 beamline
41 11.0.1.1 at the Advanced Light Source, LBNL, Berkeley, CA. Stacks of PEEM images were
42 acquired at the oxygen K-edge π^* peak energy (534 eV), while rotating the linear polarization
43 [11] to produce PIC maps using Igor Pro® (WaveMetrics, Lake Oswego, OR) and the Gilbert
44 Group (GG) Macros [66] (A.2,3). Radiation damage to the samples was not observed in any of
45 the PIC mapping experiments [58, 67-69]. Other methods like SEM, DNA, BET, μXRD , and
46 EPMA analyses are also described in Appendix A.3-A.8 and phase-field simulations in A.9.

2.1. How to read a PIC map.

Figures 2a and b show representative PIC maps of two coral skeletons across large areas, from two distantly related species: *Stylophora pistillata* (Sp) and *Balanophyllia europaea* (Be) acquired from the locations shown in the PLM images in Figures S2-S3. Colors in PIC maps, including hue and brightness, quantitatively display the azimuthal and polar angles of the *c*-axis with respect to the polarization plane, which is 60° from the image plane. The crystal *c*-axis projected onto the polarization plane is termed the *c'*-axis [11, 58], and its *c'* angle is quantitatively displayed by the hue in the color bar in Figure 2c: vertical in-plane (with respect to the polarization plane) is defined as 0° (cyan), clockwise and counterclockwise rotations from 0° are positive and negative angles, respectively, and horizontal in-plane is +90° or -90° (both red). The sample is mounted vertically, and the synchrotron x-ray beam illuminates the sample from the right at a grazing incidence angle of 30°. The polarization plane, perpendicular to the beam, is therefore rotated 60° with respect to the sample surface and intersects it along the vertical. Cyan crystals with their *c*-axes at 0°, therefore, have their *c*-axes in-plane in both the image and the polarization plane, but crystals with negative angles have *c*-axes coming out of the image plane at an angle of 60° from it and positive ones have their *c*-axes going in behind the image plane at an angle of 30°. The brightness corresponds to the off-plane angle, again with respect to the polarization plane, with 100%-brightness color indicating in-plane and 0% brightness (black) indicating 90° off-plane [58, 59]. Black crystals, therefore, have their *c*-axes directed into the beam.

2.2. Phase-field simulations.

Phase-field simulations were performed using a phase-field model that incorporates growth front nucleation (GFN) [70, 71] specially designed to describe the formation of complex polycrystalline structures in polymers and alloys as described in Appendix A.9. The model,

1
2
3
4 adopted here with modifications, describes the formation of new crystal grains, misaligned with
5 respect to the parent crystal. The frequency and orientation of GFN events is governed by the
6 relative magnitudes of the rotational and translational diffusion coefficients, D_{rot} and D_{trans} . D_{rot}
7 determines how easy it is for a molecular unit to rotate around its axis and is associated with the
8 geometry of the molecular unit, whereas D_{trans} determines how easy it is for the molecular unit to
9 travel through the liquid medium towards the growth front. Therefore, the ratio of D_{rot}/D_{trans}
10 determines how misaligned the molecular unit is when it arrives at the growth front and
11 solidifies. Accordingly, high D_{rot}/D_{trans} ratio results in epitaxial growth, whereas low D_{rot}/D_{trans} ratio
12 results in randomly oriented grains as shown in [Appendix A.9.3](#) and [Figure A.9](#).

24 **3. Results and Discussion.**

27 **3.1 Expected aragonite spherulite structures in PIC maps.**

29 In *Sp* (see [Table 1](#) for this and all other coral species abbreviations) bulk skeletons, aragonite
30 crystal fibers form spherulitic bundles, as shown in [Figure 2a](#). In each spherulite bundle, acicular
31 crystal fibers always have their *c*-axis oriented along the long axis of the crystal, and adjacent
32 crystal fibers are always only slightly misoriented with respect to their neighboring fibers, with
33 angular distance of *c*-axes across grain boundaries smaller than 35°, which is a characteristic of
34 spherulites, and in PIC maps corresponds to similar colors in adjacent fibers ([Fig. 2a](#)). The
35 CoCs appear nanoparticulate and exhibit similar adjacent colors. Abrupt color changes,
36 therefore, are only observed at the boundaries of two spherulitic bundles ([Fig. 2a](#)). In [Figure 2a](#)
37 the fibers labeled “F” are red, cyan, or magenta, indicating that their *c*-axes are nearly
38 perpendicular to the image plane, parallel to it and vertical, or parallel and rotated in-plane,
39 respectively. Even where the fibers do not appear elongated, e.g. the red fibers labeled F in
40 [Figure 2a](#), they are indeed elongated, but observed here in cross-section. All other 11 species
41 had similar spherulitic structures to *Sp* in their skeletons ([Figs. 3-6](#) and [Figs. S2-S5](#)). Thus,
42 fibers in coral skeletons are spherulitic, and their *c*-axes are invariably oriented along the long
43
44
45
46
47
48
49
50
51
52
53
54
55
56
57
58
59
60
61
62
63
64
65

1
2
3
4 axis of the fiber, as expected from extensive morphological studies [16, 26, 27, 29-31, 39, 72-
5
6 74] as well as crystal orientation ones [11, 12, 53, 75].

9 **3.2 Characterization of randomly oriented crystals termed “sprinkles”.**

10
11 In addition to spherulitic fibers and CoCs, *Be* shows crystals with abrupt change of colors across
12
13 grain boundaries, interspersed with spherulitic crystal fibers, and ranging in size between 0.2 –
14
15 20 μm , (Fig. 2b). We termed these crystals “sprinkles”, as they are reminiscent of colorful sugar
16
17 sprinkles on cupcakes. Sprinkles are equant, that is, not elongated, untextured, and randomly
18
19 oriented with respect to their neighboring grains. The angular distance of *c*-axes (Δc) across
20
21 grain boundaries is narrowly distributed for spherulitic crystal fibers ($\Delta c = 0^\circ\text{-}35^\circ$), but randomly
22
23 distributed for sprinkles ($\Delta c = 0^\circ\text{-}90^\circ$), as shown in Figures 2d,e. Multiple areas per sample, and
24
25 several samples of *Sp* and *Be* from different skeletons were analyzed, all confirming that the
26
27 results in Figure 2 are representative and reproducible.

31 **3.2.1 Sprinkles are observed in coral skeletons of 7 out of 12 coral species.**

32
33 To determine whether sprinkles are unique to *Be* or common to other species, we examined
34
35 additional coral skeletons from different coral clades (robust or complex)[76], different growth
36
37 morphologies (branching, solitary, encrusting, table-like, or massive), and of different geographic
38
39 origins (Indo-Pacific, Red Sea, and Mediterranean Sea). The 12 species analyzed are listed in
40
41 Table 1, along with the abbreviation of their genus and species, their clade, morphology,
42
43 geographical origins, and climates. The phylogenetic tree for all 12 species is presented in
44
45 Figure S1.

46
47
48
49 Out of the 12 species analyzed, 7 species exhibited sprinkles. Of these, 3 exhibited only small
50
51 sprinkles (0.2-2.0 μm , *Pam*, *Op*, *Ap*) (Fig. 3), 2 showed only large sprinkles (2-20 μm , observed
52
53 in *Mp*, *Fs*) (Fig. 4), and 2 showed both small and large sprinkles (*Be*, *Bm*)(Figs. 2b, 3, and 4).
54
55 Small and large sprinkles, e.g. the ones indicated by arrows in Figs. 3 and 4, have very different
56
57 colors at their boundaries, e.g. complementary colors such as red and cyan, or green and
58
59

1
2
3
4 magenta, or blue and yellow, thus they are misoriented sprinkles. Five out of 12 species showed
5
6 no sprinkles, or so few that they could not be unambiguously interpreted as sprinkles: they could
7
8 have been fibers from other spherulites either in front or behind the analyzed polished surface.
9
10 The species with no sprinkles include *Sp*, *Tp*, *Pl*, *Mt*, and *Ml* (Fig. 5).

11 12 13 **3.2.2 Sprinkles are equant and are not fibers from other spherulites.**

14
15 We stress that sprinkles in *Be*, *Bm*, *Pam*, *Op*, *Ap*, *Mp* and *Fs* are never elongated, therefore
16
17 they must be approximately equant, unlike the fibers that are always elongated. If sprinkles
18
19 were elongated, observing thousands of them as presented here (Figs. 2b, 3, 4 and others)
20
21 should show at least a few with their long axis randomly oriented but lying in plane and thus
22
23 appearing elongated. Since such randomly oriented, elongated crystals never appeared in any
24
25 of the PIC maps, we conclude that sprinkles are equant.
26
27

28
29 Furthermore, since the sprinkles observed in *Be*, *Bm*, *Pam*, *Op*, and *Ap* are randomly oriented,
30
31 they cannot be fibers from other spherulites in front or behind the image plane. If they were,
32
33 they would have colors different from the main spherulite imaged, but similar to one another.
34
35 The observed random distribution of colors (e.g. Fig. 2e) implies that, if sprinkles were fibers
36
37 from other spherulites, they would have to belong to tens of different spherulites, which is
38
39 geometrically impossible.
40
41

42
43 In a few PIC maps, a small set of differently oriented crystals do appear at the boundaries
44
45 between two spherulite bundles of fiber crystals (e.g. arrows in *Pl*, *Mt*, *Ml* Figs. 5d,e,f). These
46
47 sprinkles are so few that they could be from 1 or 2 other spherulites in front or behind the image
48
49 plane. We therefore conservatively placed *Pl*, *Mt*, *Ml* in the sprinkle-free group.
50

51 52 **3.2.3 Sprinkles are made of aragonite, with higher Na and Mg.**

53
54 Powder X-ray diffraction (XRD) analysis of bulk *Be* skeletons (Fig. S6) and X-ray absorption
55
56 near edge structure (XANES) spectroscopy at the Ca L-edge acquired selectively from sprinkles
57
58
59
60
61
62
63
64
65

1
2
3
4 and fibers in *Be* skeletons (Fig. S7) and fibers in *Sp* skeletons identified aragonite as the sole
5 crystalline polymorph in sprinkles and fibers alike [58].

6
7
8 Electron Probe MicroAnalysis (EPMA), however, showed that sprinkles contain significantly
9 more Na and Mg, and less Sr than spherulitic crystal fibers (Table S1). The higher amount of Mg
10 and therefore Mg/Ca ratio has been observed before in the CoCs of various coral species [77-
11 79], and may be associated with organics, an amorphous phase [80], or increased local pH [81].
12 Under the experimental conditions employed here, sprinkles are identified as fully crystalline
13 aragonite, and thus the local variation in Mg incorporation may be related to the presence of
14 different concentrations of intracrystalline Mg-binding macromolecules [21].

15
16
17
18
19
20
21
22
23
24 Synchrotron X-ray micro-diffraction (μ XRD), done in monochromatic powder diffraction mode,
25 showed that in the aragonite $\{111\}$ family of planes, the d -spacing is $0.05 \pm 0.02\%$ larger in
26 sprinkles than in spherulitic fiber crystals (Fig. S8), which is also consistent with the presence of
27 organics in sprinkle aragonite [82]. Because all *Ap* skeletons have sprinkles only at CoCs (Fig.
28 3d, 6) and the vertical black line in Figure S8 is definitely a line of CoCs, we can confidently
29 interpret the μ XRD data transect as spanning spherulitic fibers on the left, CoC-sprinkles, and
30 again fibers on the right.

3.2.4 Sprinkles are not easily recognizable in SEM images.

31
32
33
34
35
36
37
38
39
40
41
42 In all previous studies of coral skeletons from all species, the skeletons were observed to grow
43 as spherulites, thus the observation of a different non-spherulitic structure, the sprinkles, was
44 unexpected. Interestingly, SEM images of etched mature *Be* skeletons, such as those in Figure
45 S9, show spherulitic crystals, and where crystals are not acicular and radially distributed, the
46 parsimonious interpretation is that they are still spherulitic and acicular but oriented
47 perpendicular to the imaging plane. It is also possible that, because the small sprinkles are 0.2-
48 2.0 μ m, they could be mistaken for fragmented fibers in fractured samples, or they could be
49 dissolved preferentially in partially etched samples. It is therefore not surprising that previous
50
51
52
53
54
55
56
57
58
59
60
61
62
63
64
65

1
2
3
4 reports, based solely on morphological studies of sectioned, fractured, or etched coral
5 skeletons, did not describe sprinkles. The results presented here, in contrast, demonstrate that
6 crystal orientation analysis is useful to identify sprinkles and distinguish them from off-plane
7 sectioned spherulites.
8
9

10 11 12 **3.2.5 Can sprinkles be fusiform crystals?**

13
14
15 Previous SEM studies of coral skeleton growth described “fusiform crystals” in a variety of
16 species, including *Acropora cervicornis* [83], *Pocillopora damicornis* [84, 85], *Galaxea*
17 *fascicularis* [86, 87], and *Sp* [88]. These were 0.3-3 μm spindle-shaped crystals, observed at the
18 surface of the growing skeleton, and interpreted as early-stage depositions in coral skeleton
19 formation, distinct from acicular aragonite crystal fibers [83]. Although their size is similar to the
20 small sprinkles found in PIC maps, fusiform crystals were never reported to appear in the bulk of
21 mature coral skeletons, thus they may or may not be sprinkles. Sprinkles never appear fusiform
22 in shape, so it is difficult to conclude with certainty that fusiform crystals become sprinkles, once
23 they are incorporated into the growing skeleton. But their equant, random shape may be due to
24 their observation here within the skeleton, and therefore at a later developmental stage.
25
26
27
28
29
30
31
32
33
34
35
36

37 **3.2.6 Sprinkles are not CoCs, in general, but are CoCs in *Acropora*.**

38
39
40 The small sprinkles observed in *Be*, *Pam*, *Op* cannot be CoCs, because acicular crystal fibers
41 radiating from them were never observed. Furthermore, in most species, wherever CoCs were
42 recognizable by their characteristic nanoparticulate structure and by the fibers radiating from
43 them, CoC nanocrystals were not randomly oriented, but rather, neighboring crystals had similar
44 orientations (Figs. 2a, 3e, 4c,e, 5b,c,d,e).
45
46
47
48
49
50

51 In one species only, *Ap*, randomly oriented sprinkles were co-localized with CoCs (Fig. 3d, 6),
52 they were arranged along lines, and fibers radiated from sprinkles instead of CoCs. One could,
53 therefore, conclude that sprinkles are the first nucleated crystals, and occur only at the CoCs,
54 but this interpretation does not hold for the other 11 species analyzed here.
55
56
57
58
59
60
61
62
63
64
65

1
2
3
4
5
6
7
8
9 **3.2.7 Sprinkles are at the growth front (GF) of spherulitic bundles in *Be* and *Op*.**

10 In all species, sprinkles are interspersed with spherulitic crystal fibers. They are observed in
11 distantly related species, therefore, they are a broadly occurring crystal growth mode in coral
12 skeletons. In two regions of *Be* and *Op* skeletons, sprinkles appear to be layered around the GF
13 of fanning spherulitic fiber crystals (Figs. 3c,e, between pairs of GF labels). This observation is
14 consistent with GFN of sprinkles, which then either become fibers or are trapped as sprinkles,
15 as described below.
16
17
18
19
20
21
22
23

24 **3.3 Concentric rings in *Acropora*.**

25 In addition to sprinkles, spherulitic fibers, and CoCs, the *Ap* skeleton showed a fourth micro-
26 scale structure – concentric rings approximately 5 – 20 μm apart, labeled “R” in Fig. 6a and
27 magnified in Fig. 6b. Among the 12 species analyzed here, these concentric rings were only
28 observed in *Ap*, and while these features were previously described in other *Acropora* species,
29 they have not yet been fully characterized [36, 89, 90].
30
31
32
33
34
35
36
37

38 The concentric rings are composed of elongated slightly misoriented nanocrystals, as confirmed
39 by the distribution of Δc in Figure 2d, and thus, according to the quantitative definition
40 introduced by Sun *et al.* [11] they are spherulitic. However, unlike previously known spherical or
41 plumose spherulites that form fanning bundles of fibers (Fig. 2a, and middle of Fig. 6a), they
42 instead form curved layered structures. From the literature, these concentric rings are likely
43 cross-sections of small protrusions on the skeleton surface, termed “spiniform trabeculae” [89]
44 or “shingles” [36]. Interestingly, unlike spherulitic crystals fanning from CoCs, the nanocrystal
45 domains in the concentric rings do not seem to coarsen as they grow, further confirming that the
46 concentric rings are a distinct structure compared to plumose spherulite fibers radiating out of
47 CoCs.
48
49
50
51
52
53
54
55
56
57
58
59
60
61
62
63
64
65

1
2
3
4 **3.4 Coral skeleton are completely space-filling.**
5

6 To measure whether or not coral skeletons are space-filling, and if so, how much, we used the
7 Brunauer-Emmett-Teller (BET) method [91, 92]. As shown in Table 2, the specific surface area
8 of powdered coral skeletons from *Sp* and *Be* indicates that they are as space-filling as single
9 crystals of geologic aragonite.
10

11
12
13
14
15 **3.5 Hypothesis: sprinkles are proto-fibers.**
16

17 Since sprinkles formed in distantly related species are identical in mineral phase to spherulitic
18 crystal fibers, and are interspersed with fibers, we tested the hypothesis that sprinkles are proto-
19 fibers, that is, that they are the first-nucleated seed of each crystalline fiber in a spherulite, and
20 that the existence of sprinkles involves thermodynamic and kinetic controls of the crystallization
21 process during coral biomineralization.
22

23 In coral skeletons as well as other spherulitic crystal systems, the nanoscale mechanism by
24 which a new, differently oriented crystal is nucleated and then either grows or shrinks remains
25 unknown (questions c. and d), despite recent efforts [93]. New nucleation events, however, must
26 occur all the time during spherulitic growth, not only at the center of a sphere or at the CoCs, but
27 everywhere, in order to fill space. Otherwise, acicular crystals would diverge from one another
28 as spokes on a wheel, with increasingly large gaps between crystals. This is never the case in
29 spherulites, whether biogenic (see Table 2 and [92]), geologic, or synthetic: spherulites are
30 always space-filling.
31

32 We propose that randomly oriented crystals, such as the sprinkles observed here, solve this
33 problem: they are the first-nucleated, initially randomly oriented seeds of fiber crystals, which, if
34 they are nearly co-oriented with their neighboring crystals, have space to grow larger radially, if
35 not, they do not, run into one another during growth and remain smaller. In the first case, the
36 sprinkle is a proto-fiber, in the second it is mis-oriented. We tentatively propose that a
37 coarsening process makes small, mis-oriented sprinkles disappear. Occasionally, in 7 of the 12
38
39
40
41
42
43
44
45
46
47
48
49
50
51
52
53
54
55
56
57
58
59
60
61
62
63
64
65

1
2
3
4 coral species, either the organics likely trapped in sprinkles, or other mechanisms, stabilize the
5
6 sprinkles and make them resist the coarsening process, which, we further hypothesize, occurs
7
8 spontaneously, and is therefore common to biogenic, geologic, and synthetic spherulitic growth.
9
10 The randomly oriented sprinkle seeds observed here do not nucleate in any mechanism
11
12 previously observed or simulated. In the data presented, sprinkles are frequently nucleated at all
13
14 distances from spherulite centers, the CoCs, thus **a mechanism** that includes and explains their
15
16 existence is necessary.
17
18

19 **3.6 Growth front nucleation (GFN) in coral skeletons.**

20
21 The sprinkles observed in *Be* and *Op* are preferentially localized along growth fronts as
22
23 presented in **Figs. 3c,e**. This suggests that GFN occurs in coral skeletons, and that sprinkles are
24
25 the first nucleated crystals at the GF. The main technique used to model GFN in this paper is
26
27 phase-field simulation using a phase-field model incorporating GFN [70, 71], briefly described in
28
29 section 2.2 and in greater detail in **Appendix A.9**.
30
31

32 **3.7 Proposed spherulitic growth mechanism: GFN of sprinkles.**

33
34 Based on the observation of sprinkles at GFs, and the hypothesis that sprinkles are proto-fibers,
35
36 here we propose **a mechanism** for the growth of spherulites that includes and explains
37
38 sprinkles. **The mechanism** of spherulite growth we propose is summarized in **Figure 7**, and it
39
40 has four stages:
41
42

- 43
44 1. Randomly oriented sprinkles nucleate from a liquid or an amorphous solid, immediately
45
46 outside the liquid-solid interface or inside of it at the expense of an amorphous precursor solid
47
48 [94]. In corals, the interface is the surface of the growing coral skeleton, and nucleation of
49
50 sprinkles occurs within the amorphous solid, near the surface, but inside of it by a few microns.
51
52

53 **Fig. S10** substantiates this expectation.
54
55
56
57
58
59

1
2
3
4 2. Aragonite crystals, or any other spherulite-forming crystals, grow preferentially along the
5 *c*-axis, thus the aspect ratio of sprinkle nuclei increases, and the crystals become acicular. In
6 corals skeletons, they become fibers, which grow at the expense of the amorphous precursors.
7
8

9
10 3. During this growth, sprinkles with their *c*-axes radially oriented have space to elongate,
11 whereas transverse ones run into one another and thus remain small. The result is spherulitic
12 growth of acicular crystal fibers with slight misorientation across grain boundaries. This growth
13 mechanism concurs with Barnes's competition for space model [16], and with Gladfelter's
14 hypothesis that randomly oriented fusiform crystals are the first to be deposited [83]. The latter
15 concurs with sprinkles, if fusiform crystals and sprinkles are the same entities. The nucleation
16 and space filling of sprinkles and fibers concur with the classical understanding of polycrystalline
17 3D-solid or 2D-film formation [95].
18
19

20 4. Finally, sprinkles with their *c*-axes radially oriented grow into larger fibers and other non-
21 radially oriented sprinkles shrink. In this coarsening process, radial sprinkles grow at the
22 expense of non-radial, smaller ones. In corals, the coarsening process occurs in the bulk of the
23 skeleton, once all or most of the skeleton has solidified and filled space. If the skeleton surface
24 is not yet space-filling, but still porous at the time of coarsening, the calcifying fluid between the
25 cells and the growing skeleton [96] may facilitate the dissolution and re-precipitation of smaller
26 sprinkles and coarsening of the larger, radially oriented ones [97, 98]. If it is already space-
27 filling, then coarsening could be an entirely solid-state transformation, akin to the coarsening of
28 polycrystalline metals such as Ag and Pt that can occur at room temperature [99, 100].
29 Coarsening in liquid or solid phases is well-established in classical crystallization, and usually
30 termed Ostwald ripening [97, 98] or Smoluchowski ripening [99, 100], respectively.
31
32

33 During coarsening, small sprinkles shrink and disappear, whereas spherulitic crystals grow
34 larger. This mechanism explains why random orientations are usually not observed in
35
36
37
38
39
40
41
42
43
44
45
46
47
48
49
50
51
52

1
2
3
4 spherulites: by the time a spherulite is fully formed and coarsened, it no longer contains
5
6 sprinkles. Occasionally, however, sprinkles are retained.

7
8 Such a thermodynamically driven skeletal growth process has been described in *Pinna nobilis*
9
10 prismatic calcite [101], whose grains coalesce according to classical metallurgical theory [102],
11
12 or in the aragonitic shells of *Unio pictorum*, *Nautilus pompilius*, and *Haliotis asinina*, whose
13
14 ultrastructure gradually transitions from a randomly aggregated, to a prismatic, to a nacre layer,
15
16 through a directional solidification process [103, 104], as occurs in metals.
17
18

19 20 **3.8 Compatibility with amorphous precursors.**

21
22 It is known that coral skeletons grow at the expense of amorphous precursors [94]. The space-
23
24 filling of sprinkles and fibers discussed here, and their coarsening, are invariant whether the
25
26 crystals grow at the expense of ions from solution, a dense liquid precursor, or a space-filling
27
28 solid amorphous precursor. The concepts proposed here are purely geometric, and thus not
29
30 affected by these three distinct scenarios for coral skeleton formation. Nucleation and growth
31
32 throughout this paper refer to a new crystal orientation, not to an amorphous solid nucleating
33
34 and growing from liquid solution.
35
36

37 38 **3.9 Phase-field simulations support the proposed formation from proto-fiber sprinkles.**

39
40 To test the hypothesis that sprinkles are the first nucleated crystals at the GF, and that they grow
41
42 and coarsen if they are radially oriented but are sometimes retained as observed in coral
43
44 skeletons, we performed a phase-field simulation in which sprinkles are deposited first, and then
45
46 grow competitively. We used the spherulite model in Gránásy et al. [105], but omitted the local
47
48 minimum in grain boundary energy that would force GFN with a given misorientation, and would
49
50 thus yield a fixed mis-orientation angle. In our simulation, therefore, GFN of sprinkles occurs
51
52 with random orientation. The simulations were performed in two dimensions, and we applied a
53
54 large two-fold symmetry for the solid-liquid interface energy, which yields elongated growth
55
56 shapes mimicking aragonite crystals. Remarkably, not only did the crystals in the simulations
57
58
59

1
2
3
4 grow into a spherulite with small grain boundary angles, but there were also sprinkles scattered
5 within the spherulite, as shown in [Figure 8](#). With time, some of the sprinkles formed during GFN
6 remained sprinkles ([Fig. 8](#), white boxes), whereas others disappeared due to competitive grain
7 coarsening ([Fig. 8](#), black boxes). Both observations are consistent with the PIC mapping data
8 presented here for coral skeleton spherulitic fibers and sprinkles. The coarsening, proposed and
9 tested here, could involve dissolution and recrystallization of the sprinkles at the solid-liquid
10 interface, but could also happen within the solid, where shrinking grains minimize surface
11 energy (Ostwald or Smoluchowski ripening). Grain boundaries are disordered, in the phase-field
12 simulation they are regions with higher, liquid-like mobility, and thus facilitate re-orientation of
13 the units at the periphery of a sprinkle as the sprinkle shrinks and eventually disappears. In the
14 case of coral skeletons, the re-orientation of sprinkles can occur as dissolution and
15 reprecipitation from the calcifying fluid, and Ostwald ripening, or as grain shrinking, enabled by
16 the sparing amount of water released by dehydration of hydrated amorphous calcium carbonate
17 nanoparticles. Such hydrated nanoparticles are present in the forming skeleton and surrounded
18 by crystalline aragonite, as shown by Mass et al. [\[94\]](#)

19
20 In a previous study, Sun et al. analyzed aragonite spherulites synthesized at room temperature
21 and 1 atm in the absence of any organic molecules, and never found any sprinkles [\[11\]](#). Thus,
22 the D_{rot} of aragonitic CaCO_3 molecular units typically falls in a range that allows certain
23 frequencies and misalignments of GFN to favor spherulitic structures to form at ambient
24 conditions. For sprinkles to persist, instead, D_{rot} must be smaller, so sprinkles can form via GFN
25 without matching their orientations to the mother crystal. Such small D_{rot} could be induced by
26 binding of organic molecules to CaCO_3 molecules or particles, and/or the presence of trace
27 element impurities. This possibility is supported by the fact that electrophoretic analyses of coral
28 skeletal organic matrices [\[19, 106\]](#) exhibit variability between species. The size and shape of

1
2
3
4 spherulitic aragonite crystals also varies across different taxa and species [22, 107]. Thus, in
5
6 different coral species D_{rot} is likely different.

9 **3.10 Simulations support all of the experimentally observed structures.**

10 In summary, the theoretical phase-field simulation in Figure 8 shows strong similarity with the
11
12 proposed mechanism: small sprinkles originate through GFN, then recrystallize in a coarsening
13
14 process and thus, we argue, are not observed in many coral skeletons (Fig. 5, *Sp*, *Tp*, *Pl*, *Mt*,
15
16 *Ml*) presumably because these have a larger D_{rot}/D_{trans} ratio. Coral skeletons that retain small
17
18 sprinkles (Fig. 3, *Bm*, *Pam*, *Op*, *Ap*, *Be*), instead, presumably have a smaller D_{rot}/D_{trans} ratio. A
19
20 variety of such D_{rot}/D_{trans} ratios is presented in Appendix A, Figure A.9.

21
22
23
24 The simulation of Figure 9a shows that a branched structure can grow, in which the center of
25
26 each branch resembles *Ap* coral skeletons (Figs. 2d, 6, 9, S5, S8, S11) with sprinkles along
27
28 CoCs, whereas the larger crystals on the outside of each branch are similar to the large
29
30 sprinkles (2-20 μm) observed in some skeletons (Fig. 4, *Bm*, *Mp*, *Fs*, *Be*). The simulations
31
32 presented here, therefore, are able to reproduce all the observed structural features found in
33
34 real coral skeletons.

37 **3.11 Additional support for GFN of sprinkles in fresh, forming *Stylophora pistillata*.**

38
39 In addition to theoretical simulations, an independent line of evidence suggests initial GFN of
40
41 sprinkles: Figure S10 shows that, near the surface of *Sp* skeletons, randomly oriented sprinkles
42
43 can be retained. These were only observed in fresh forming skeletons near the growth front,
44
45 whereas in the mature *Sp* skeletons, only spherulitic crystal fibers and CoCs were found (Figs.
46
47 2a, 5c). The presence of sprinkles near the GF in a fresh, forming *Sp* coral skeleton (Fig. S10)
48
49 and their absence in the mature *Sp* skeletons (Figs. 2a,5c) is the only experimental evidence
50
51 that sprinkles disappear, and is only indirect evidence.

55 **3.12 Possible relevance to other biomineral systems.**

1
2
3
4 Other biominerals have been previously observed to have nearly co-oriented neighboring
5 crystals, including mollusk shell nacre [108] and calcite prisms [109], and ascidian (tunicate)
6 spicules [59]. The growth mechanism described here, including competition for space and
7 coarsening, may be relevant to other geometries, completely different from spherulitic crystals.
8
9 But this must be demonstrated in future work, beyond the scope of the present paper. The same
10 growth mechanism may also apply to biomimetic spherulites [110].
11
12
13
14
15
16
17
18
19
20
21

22 **3.13 Possible relevance to semicrystalline polymers.**

23
24 A variety of organic macromolecules or polymers used to make plastics, rubber, textiles etc., are
25 partly crystalline and partly amorphous, and are therefore termed semicrystalline. The
26 crystalline component is frequently spherulitic [111]. The degree of crystallinity, that is, what
27 proportion of the polymers, after solidification, are crystalline and not amorphous is inversely
28 proportional to the molecular weight of the polymers [112-114], as longer polymer chains are
29 harder to fully crystallize. Raman spectroscopy is highly sensitive to the degree of crystallinity in
30 bulk polymer materials [115-117], but it is most commonly employed for bulk analysis. Using
31 spatially resolved Raman spectroscopy, Yang et al. recently studied the degree of crystallinity
32 within single spherulites. They found that crystallinity is not evenly distributed, but lower near the
33 center of each spherulite and increases with position along the spherulite radius [118]. The
34 pattern of crystallinity thus has important implications for the melting point and the glass
35 transition temperature of the polymer materials.
36
37
38
39
40
41
42
43
44
45
46
47
48
49
50

51 The mechanism tentatively proposed here may therefore also be relevant to semicrystalline
52 polymer materials. In this case, the first-nucleated crystals would be randomly oriented polymer
53 sprinkles, followed by crystal growth in competition for space, and coarsening. Arresting
54
55
56
57
58
59
60
61
62
63
64
65

1
2
3
4 coarsening, perhaps through rapid freezing, may reveal sprinkles, detectable by Raman
5 spectroscopy and visible by PLM.
6
7

8
9 In mesocrystalline polymer films, sprinkles are occasionally observed, interspersed with acicular
10 spherulitic crystals (see figure 2B in ref. [95]). The acicular crystals grow and surround sprinkles,
11 exactly as they do in coral skeletons (e.g. Fig. 2b arrows).
12
13
14

15 **4. Conclusions.**

16
17
18 In summary, we analyzed the skeletons of 12 distantly related coral species and a key feature
19 emerged: 7 of the 12 species exhibit 0.2-20 μm randomly oriented sprinkles. Even sprinkle-free
20 corals, however, showed sprinkles near the skeletal growth front, and in all species examined,
21 no correlation was found between the formation of sprinkles and either environmental factors or
22 evolutionary history. The observation of sprinkles suggested a growth mechanism for
23 spherulites, in which sprinkles are formed by randomly oriented GFN events, competition for
24 space, and coarsening, and not through slightly misoriented nucleations as previously assumed
25 for NCB. This mechanism is strongly supported by phase-field simulations, which explain the
26 microstructural variations across species in terms of thermodynamic parameters, and their
27 possible origin from differences in matrix organic molecules or trace element composition. In
28 addition to providing new insights into the coral biomineralization processes, this study may
29 prove useful for spherulitic crystal growth in general, which occurs in many other systems
30 including aspirin [119, 120], polymers [118], shrimp eyes [121], opal [122], graphite in cast iron
31 [123], and cocoa butter in chocolate [124]. Thus, the spherulite formation mechanism proposed
32 here may be applied to mineral and organic spherulites, natural and synthetic crystals, in the
33 metallurgical, pharmaceutical, and food industries. Furthermore, this study provides evidence
34 that interdisciplinary research combining experimental and theoretical techniques can be a
35 particularly powerful approach for elucidating the fundamental mechanisms of crystal nucleation
36 and growth.
37
38
39
40
41
42
43
44
45
46
47
48
49
50
51
52
53
54
55
56
57
58
59
60
61
62
63
64
65

5. Appendices

Appendix A.1-9: Detailed Materials and Methods.

Appendix B: Figures S1–S11, Tables S1–S2.

6. Acknowledgements

We thank Andreas Scholl for his technical help during beamtime, Franklin Hobbs during powder XRD, John Fournelle for EPMA analysis, Carl I. Steefel and Wenming Dong for BET analysis. This work was 80% supported by the U.S. Department of Energy, Office of Science, Office of Basic Energy Sciences, Chemical Sciences, Geosciences, and Biosciences Division [Award DE-FG02-07ER15899 to PG], and 20% by NSF [grant DMR-1603192 to PG]. In addition, TM acknowledges support from the United States-Israel Binational Science Foundation [BSF Grant # 2014035], and from the European Research Commission [ERC Grant # 755876]. GF and SG thank the European Research Council under the European Union's Seventh Framework Programme [FP/2007-2013, ERC; Grant # 249930 – CoralWarm]. LG and TP acknowledge the support by the National Agency for Research, Development, and Innovation, Hungary [NKFIH Contracts No. KKP-126749 and K-115959]. All PIC maps were acquired at the Advanced Light Source, which is supported by the Director, Office of Science, Office of Basic Energy Sciences, US Department of Energy [Contract No. DE-AC02-05CH11231].

7.

- [1] N.N. Geveling, S.B. Maslenkov, Solidification of eutectic Ni-Ni₃Ti alloys, *Metal Sci Heat Treatm* 18(9) (1976) 755-760.
- [2] F.J. Padden, H.D. Keith, Spherulitic crystallization in polypropylene, *J Appl Phys* 30(10) (1959) 1479-1484.
- [3] A. Shtukenberg, J. Freundenthal, E. Gunn, L. Yu, B. Kahr, Glass-crystal growth mode for testosterone propionate, *Cryst Growth Des* 11(10) (2011) 4458-4462.
- [4] A.G. Shtukenberg, C.T. Hu, Q. Zhu, M.U. Schmidt, W. Xu, M. Tan, B. Kahr, The third

References

- ambient aspirin polymorph, *Cryst Growth Des* 17(6) (2017) 3562-3566.
- [5] J. Way, J. Atkinson, J. Nutting, The effect of spherulite size on the fracture morphology of polypropylene, *J Mater Sci* 9(2) (1974) 293-299.
- [6] A.D. Fowler, B. Berger, M. Shore, M.I. Jones, J. Ropchan, Supercooled rocks: development and significance of varioles, spherulites, dendrites and spinifex in Archaean volcanic rocks, Abitibi Greenstone belt, Canada, *Precambrian Res* 115(1–4) (2002) 311-328.
- [7] A.S. Peloquin, P. Verpaerst, J.N. Ludden, Spherulitic rhyolites of the Archean Blake River

1
2
3
4 Group, Canada; implications for stratigraphic
5 correlation and volcanogenic massive sulfide
6 exploration, *Econ Geol* 91(2) (1996) 343-354.

7 [8] M.T. Hincke, Y. Nys, J. Gautron, The
8 eggshell: structure, composition and
9 mineralization, *Front Biosci* 17(1266) (2012)
10 120.

11 [9] E. Parmentier, R. Cloots, R. Warin, C.
12 Henrist, Otolith crystals (in Carapidae): Growth
13 and habit, *J Struct Biol* 159(3) (2007) 462-473.

14 [10] U. Al-Atar, A.A. Bokov, D. Marshall,
15 J.M.H. Teichman, B.D. Gates, Z.-G. Ye, N.R.
16 Branda, Mechanism of calcium oxalate
17 monohydrate kidney stones formation: layered
18 spherulitic growth, *Chem Mater* 22(4) (2010)
19 1318-1329.

20 [11] C.Y. Sun, M.A. Marcus, M.J. Frazier, A.J.
21 Giuffre, T. Mass, P. Gilbert, Spherulitic growth
22 of coral skeletons and synthetic aragonite:
23 Nature's three-dimensional printing, *ACS Nano*
24 11(7) (2017) 6612-6622.

25 [12] K. Benzerara, N. Menguy, M. Obst, J.
26 Stolarski, M. Mazur, T. Tylicszak, G.E. Brown,
27 Jr., A. Meibom, Study of the crystallographic
28 architecture of corals at the nanoscale by
29 scanning transmission X-ray microscopy and
30 transmission electron microscopy,
31 *Ultramicroscopy* 111(8) (2011) 1268-75.

32 [13] J.H. Magill, Review spherulites: a personal
33 perspective, *J Mat Sci* 36(13) (2001) 3143-3164.

34 [14] W.H. Bryan, D. Hill, Spherulitic
35 crystallization as a mechanism of skeletal
36 growth in the hexacorals, *Procs R Soc*
37 *Queensland LII*(9) (1941) 78-91.

38 [15] M.M. Ogilvie, Microscopic and systematic
39 study of madreporarian types of corals, *Phil*
40 *Trans R Soc London. Series B* 187 (1896) 83-
41 345.

42 [16] D.J. Barnes, Coral Skeletons: An
43 Explanation of Their Growth and Structure,
44 *Science* 170(3964) (1970) 1305-1308.

45 [17] A. Akiva, M. Neder, K. Kahil, R. Gavriel, I.
46 Pinkas, G. Goobes, T. Mass, Minerals in the pre-
47 settled coral *Stylophora pistillata* crystallize via
48 protein and ion changes, *Nat Comms* 9(1)
49 (2018) 1880.

50 [18] T. Mass, J.L. Drake, E.C. Peters, W. Jiang,
51 P.G. Falkowski, Immunolocalization of skeletal
52 matrix proteins in tissue and mineral of the coral

Stylophora pistillata, *Procs Natl Acad Sci*
111(35) (2014) 12728-12733.

53 [19] J.-P. Cuif, Y. Dauphin, J. Doucet, M.
54 Salome, J. Susini, XANES mapping of organic
55 sulfate in three scleractinian coral skeletons,
56 *Geochim Cosmochim Acta* 67(1) (2003) 75-83.

57 [20] G. Falini, M. Reggi, S. Fermani, F. Sparla,
58 S. Goffredo, Z. Dubinsky, O. Levi, Y. Dauphin,
59 J.-P. Cuif, Control of aragonite deposition in
60 colonial corals by intra-skeletal macromolecules,
61 *J Struct Biol* 183(2) (2013) 226-238.

62 [21] R. Laipnik, V. Bissi, C.-Y. Sun, G. Falini,
63 P.U. Gilbert, T. Mass, Coral acid rich protein
64 selects vaterite polymorph in vitro, *Journal of*
65 *Structural Biology* in press. (2019) 107431.

[22] J.P. Cuif, Y. Dauphin, The two-step mode
of growth in the scleractinian coral skeletons
from the micrometre to the overall scale, *J Struct*
Biol 150(3) (2005) 319-31.

[23] M. Reggi, S. Fermani, V. Landi, F. Sparla,
E. Caroselli, F. Gizzi, Z. Dubinsky, O. Levy, J.-
P. Cuif, Y. Dauphin, S. Goffredo, G. Falini,
Biom mineralization in Mediterranean Corals: The
Role of the Intraskelletal Organic Matrix, *Cryst*
Growth Des 14(9) (2014) 4310-4320.

[24] H. Wang, A revision of the *Zoantharia*
Rugosa in the light of their minute skeletal
structures, *Phil Trans R Soc London. Series B*
234(611) (1950) 175-246.

[25] S.A. Wainwright, Studies of the mineral
phase of coral skeleton, *Exper Cell Res* 34(2)
(1964) 213-230.

[26] J.-P. Cuif, Y. Dauphin, Microstructural and
physico-chemical characterization of 'centers of
calcification' in septa of some Recent
scleractinian corals, *Paläontologische Zeitschrift*
72(3-4) (1998) 257-269.

[27] C. Rollion-Bard, D. Blamart, J.-P. Cuif, A.
Juillet-Leclerc, Microanalysis of C and O
isotopes of azooxanthellate and zooxanthellate
corals by ion microprobe, *Coral Reefs* 22(4)
(2003) 405-415.

[28] J. Stolarski, Three-dimensional micro-and
nanostructural characteristics of the scleractinian
coral skeleton: a biocalcification proxy, *Acta*
Palaeontol Polon 48(4) (2003).

[29] L.D. Nothdurft, G.E. Webb, Microstructure
of common reef-building coral genera *Acropora*,
Pocillopora, *Goniastrea* and *Porites*: constraints

1
2
3
4 on spatial resolution in geochemical sampling,
5 *Facies* 53(1) (2007) 1-26.

6 [30] C. Brahmi, A. Meibom, D. Smith, J.
7 Stolarski, S. Auzoux-Bordenave, J. Nouet, D.
8 Doumenc, C. Djediat, I. Domart-Coulon,
9 Skeletal growth, ultrastructure and composition
10 of the azooxanthellate scleractinian coral
11 *Balanophyllia regia*, *Coral Reefs* 29(1) (2010)
12 175-189.

13 [31] J.-P. Cuif, Y. Dauphin, J.E. Sorauf,
14 *Biominerals and fossils through time*,
15 Cambridge University Press 2010.

16 [32] O.H. Shapiro, E. Kramarsky-Winter, A.R.
17 Gavish, R. Stocker, A. Vardi, A coral-on-a-chip
18 microfluidic platform enabling live-imaging
19 microscopy of reef-building corals, *Nat Comms*
20 7 (2016) 10860.

21 [33] A.L. Cohen, M. Holcomb, Why corals care
22 about ocean acidification: uncovering the
23 mechanism, *Oceanography* 22(4) (2009) 118-
24 127.

25 [34] A.L. Cohen, T.A. McConnaughey,
26 *Geochemical perspectives on coral*
27 *mineralization*, *Revs Mineral Geochem* 54(1)
28 (2003) 151-187.

29 [35] M. Holcomb, A.L. Cohen, R.I. Gabitov,
30 J.L. Hutter, Compositional and morphological
31 features of aragonite precipitated experimentally
32 from seawater and biogenically by corals,
33 *Geochim Cosmochim Acta* 73(14) (2009) 4166-
34 4179.

35 [36] L.D. Nothdurft, G.E. Webb, Microstructure
36 of common reef-building coral genera *Acropora*,
37 *Pocillopora*, *Goniastrea* and *Porites*: constraints
38 on spatial resolution in geochemical sampling,
39 *Facies* 53(1) (2006) 1-26.

40 [37] B. Constantz, A. Meike, Calcite centers of
41 calcification in *Mussa angulosa* (Scleractinia),
42 Origin, evolution, and modern aspects of
43 biomineralization in plants and animals,
44 Springer 1989, pp. 201-207.

45 [38] K. Shirai, M. Kusakabe, S. Nakai, T. Ishii,
46 T. Watanabe, H. Hiyagon, Y. Sano, Deep-sea
47 coral geochemistry: Implication for the vital
48 effect, *Chemical Geology* 224(4) (2005) 212-
49 222.

50 [39] H. Wang, A revision of the *Zoantharia*
51 *Rugosa* in the light of their minute skeletal
52 structures, *Philosophical Transactions of the*
53
54
55

Royal Society of London. Series B, Biological
56 Sciences 234(611) (1950) 175-246.

57 [40] K. Ramseyer, T.M. Miano, V. D'orazio, A.
58 Wildberger, T. Wagner, J. Geister, Nature and
59 origin of organic matter in carbonates from
60 speleothems, marine cements and coral
61 skeletons, *Organic Geochem* 26(5-6) (1997)
62 361-378.

63 [41] C. Rollion-Bard, D. Blamart, SIMS method
64 and examples of applications in coral
65 biomineralization, *Biominalization*
66 *Sourcebook: Characterization of Biominerals*
67 *and Biomimetic Materials*; DiMasi, E., Gower,
68 LB, Eds (2014) 249-261.

69 [42] P. Gautret, J.-P. Cuif, J. Stolarski, Organic
70 components of the skeleton of scleractinian
71 corals-evidence from in situ acridine orange
72 staining, *Acta Palaeontol Polon* 45(2) (2000)
73 107-118.

74 [43] S. Goffredo, P. Vergni, M. Reggi, E.
75 Caroselli, F. Sparla, O. Levy, Z. Dubinsky, G.
76 Falini, The skeletal organic matrix from
77 Mediterranean coral *Balanophyllia europaea*
78 influences calcium carbonate precipitation,
79 *PLoS One* 6(7) (2011) e22338.

80 [44] K. Ramseyer, T.M. Miano, V. D'orazio, A.
81 Wildberger, T. Wagner, J. Geister, Nature and
82 origin of organic matter in carbonates from
83 speleothems, marine cements and coral
84 skeletons, *Organic Geochemistry* 26(5-6) (1997)
85 361-378.

86 [45] S. Von Euw, Q. Zhang, V. Manichev, N.
87 Murali, J. Gross, L.C. Feldman, T. Gustafsson,
88 C. Flach, R. Mendelsohn, P.G. Falkowski,
89 Biological control of aragonite formation in
90 stony corals, *Science* 356(6341) (2017) 933-938.

91 [46] E. Beniash, C.A. Stifler, C.-Y. Sun, G.S.
92 Jung, Z. Qin, M.J. Buehler, P.U.P.A. Gilbert,
93 The hidden structure of human enamel *Nat*
94 *Comms* 10 (2019) 4383/1-13.

95 [47] M.A. Marcus, S. Amini, C.A. Stifler, C.-Y.
96 Sun, M.J. Frazier, N. Tamura, H.A. Bechtel,
97 D.Y. Parkinson, H.S. Barnard, X.X.X. Zhang,
98 J.Q.I. Chua, A. Miserez, P.U.P.A. Gilbert,
99 Parrotfish teeth: stiff biominerals whose
100 microstructure makes them tough and abrasion-
101 resistant to bite stony corals, *ACS Nano* 11(22)
102 (2017) 11856-11865.

103 [48] R. van de Locht, A. Verch, M. Saunders, D.
104 Dissard, T. Rixen, A. Moya, R. Kroger,

1
2
3
4
5
6
7
8
9
10
11
12
13
14
15
16
17
18
19
20
21
22
23
24
25
26
27
28
29
30
31
32
33
34
35
36
37
38
39
40
41
42
43
44
45
46
47
48
49
50
51
52
53
54
55
56
57
58
59
60
61
62
63
64
65

Microstructural evolution and nanoscale crystallography in scleractinian coral spherulites, *J Struct Biol* 183(1) (2013) 57-65.

[49] N. Nassif, F. Martineau, O. Syzgantseva, F. Gobeaux, M. Willinger, T. Coradin, S. Cassaignon, T. Azaïs, M.-M. Giraud-Guille, In vivo inspired conditions to synthesize biomimetic hydroxyapatite, *Chemistry of Materials* 22(12) (2010) 3653-3663.

[50] J.P. Cuif, Y. Dauphin, The environment recording unit in coral skeletons – a synthesis of structural and chemical evidences for a biochemically driven, stepping-growth process in fibres, *Biogeosciences* 2(1) (2005) 61-73.

[51] I. Coronado, A. Pérez-Huerta, S. Rodríguez, Computer-integrated polarisation (CIP) in the analysis of fossils: a case of study in a Palaeozoic coral (*Sinopora*, *Syringoporicae*, Carboniferous), *Histor Biol* 27(8) (2014) 1098-1112.

[52] J. Stolarski, M. Mazur, Nanostructure of biogenic versus abiogenic calcium carbonate crystals, *Acta Palaeontol Polon* 50(4) (2005) 847-865.

[53] M. Cusack, J. England, P. Dalbeck, A.W. Tudhope, A.E. Fallick, N. Allison, Electron backscatter diffraction (EBSD) as a tool for detection of coral diagenesis, *Coral Reefs* 27(4) (2008) 905-911.

[54] V. Mouchi, P. Vonlanthen, E.P. Verrecchia, Q.G. Crowley, Multi-scale crystallographic ordering in the cold-water coral *Lophelia pertusa*, *Sci Rep* 7(1) (2017) 8987.

[55] L. Muscatine, C. Goiran, L. Land, J. Jaubert, J.-P. Cuif, D. Allemand, Stable isotopes ($\delta^{13}\text{C}$ and $\delta^{15}\text{N}$) of organic matrix from coral skeleton, *Procs Natl Acad Sci* 102(5) (2005) 1525-1530.

[56] P.U. Gilbert, S.M. Porter, C.-Y. Sun, S. Xiao, B.M. Gibson, N. Shenkar, A.H. Knoll, Biomineralization by particle attachment in early animals, *Procs Natl Acad Sci* 116 (2019) 17659–17665.

[57] P.U.P.A. Gilbert, Photoemission spectromicroscopy for the biomineralogist, in: E. DiMasi, L.B. Gower (Eds.), *Biomineralization Sourcebook, Characterization of Biominerals and Biomimetic Materials*, CRC Press 2014, pp. 135-151.

[58] R.T. DeVol, R.A. Metzler, L. Kabalah-Amitai, B. Pokroy, Y. Politi, A. Gal, L. Addadi, S. Weiner, A. Fernandez-Martinez, R. Demichelis, J.D. Gale, J. Ihli, F.C. Meldrum, A.Z. Blonsky, C.E. Killian, C.B. Salling, A.T. Young, M.A. Marcus, A. Scholl, A. Doran, C. Jenkins, H.A. Bechtel, P.U.P.A. Gilbert, Oxygen spectroscopy and polarization-dependent imaging contrast (PIC)-mapping of calcium carbonate minerals and biominerals, *J Phys Chem B* 118(28) (2014) 8449-57.

[59] B. Pokroy, L. Kabalah-Amitai, I. Polishchuk, R.T. DeVol, A.Z. Blonsky, C.-Y. Sun, M.A. Marcus, A. Scholl, P.U.P.A. Gilbert, Narrowly distributed crystal orientation in biomineral vaterite, *Chem Mater* 27(19) (2015) 6516-6523.

[60] P.U.P.A. Gilbert, K.D. Bergmann, C.E. Myers, M.A. Marcus, R.T. DeVol, C.-Y. Sun, A.Z. Blonsky, E. Tamre, J. Zhao, E.A. Karan, N. Tamura, S. Lemer, A.J. Giuffre, G. Giribet, J.M. Eiler, A.H. Knoll, Nacre tablet thickness records formation temperature in modern and fossil shells, *Earth Plan Sci Lett* 460 (2017) 281-292.

[61] G. De Stasio, M. Capozzi, G.F. Lorusso, P.A. Baudat, T.C. Droubay, P. Perfetti, G. Margaritondo, B.P. Tonner, MEPHISTO: Performance tests of a novel synchrotron imaging photoelectron spectromicroscope, *Rev Sci Instrum* 69(5) (1998) 2062-2066.

[62] L. Gránásy, G.I. Tóth, J.A. Warren, F. Podmaniczky, G. Tegze, L. Rátkai, T. Pusztai, Phase-field modeling of crystal nucleation in undercooled liquids – A review, *Progr Mat Sci* (2019) 100569.

[63] X. Cui, A.L. Rohl, A. Shtukenberg, B. Kahr, Twisted aspirin crystals, *J Am Chem Soc* 135(9) (2013) 3395-3398.

[64] A.G. Shtukenberg, Y.O. Punin, E. Gunn, B. Kahr, Spherulites, *Chem Rev* 112(3) (2012) 1805-38.

[65] G. De Stasio, B.H. Frazer, B. Gilbert, K.L. Richter, J.W. Valley, Compensation of charging in X-PEEM: a successful test on mineral inclusions in 4.4 Ga old zircon, *Ultramicroscopy* 98(1) (2003) 57-62.

[66] GG-Macros, <http://home.physics.wisc.edu/gilbert/software.htm> (2019).

- 1
2
3
4 [67] P.U.P.A. Gilbert, A. Young, S.N.
5 Coppersmith, Measurement of c-axis angular
6 orientation in calcite (CaCO₃) nanocrystals
7 using x-ray absorption spectroscopy, *Procs Natl*
8 *Acad Sci* 108 (2011) 11350-11355.
9 [68] R.T. DeVol, C.-Y. Sun, M.A. Marcus, S.N.
10 Coppersmith, S.C.B. Myneni, P.U.P.A. Gilbert,
11 Nanoscale transforming mineral phases in fresh
12 nacre, *J Am Chem Soc* 137(41) (2015) 13325-
13 13333.
14 [69] T. Parasassi, O. Sapora, A.M. Giusti, G. De
15 Stasio, G. Ravagnan, Alterations in erythrocyte-
16 membrane lipids induced by low-doses of
17 ionizing-radiation as revealed by 1,6-diphenyl-
18 1,3,5-hexatriene fluorescence lifetime, *Int J Rad*
19 *Biol* 59(1) (1991) 59-69.
20 [70] L. Gránásy, T. Pusztai, T. Börzsönyi, J.A.
21 Warren, J.F. Douglas, A general mechanism of
22 polycrystalline growth, *Nat Mater* 3(9) (2004)
23 645-50.
24 [71] L. Gránásy, T. Pusztai, G. Tegze, J.A.
25 Warren, J.F. Douglas, Growth and form of
26 spherulites, *Phys Rev E* 72(1) (2005) 011605.
27 [72] S.A. Wainwright, Studies of the mineral
28 phase of coral skeleton, *Experimental Cell*
29 *Research* 34(2) (1964) 213-230.
30 [73] J. Stolarski, Three-dimensional micro-and
31 nanostructural characteristics of the scleractinian
32 coral skeleton: a biocalcification proxy, *Acta*
33 *Palaeontologica Polonica* 48(4) (2003).
34 [74] O.H. Shapiro, E. Kramarsky-Winter, A.R.
35 Gavish, R. Stocker, A. Vardi, A coral-on-a-chip
36 microfluidic platform enabling live-imaging
37 microscopy of reef-building corals, *Nature*
38 *communications* 7 (2016) 10860.
39 [75] V. Mouchi, P. Vonlanthen, E.P. Verrecchia,
40 Q.G. Crowley, Multi-scale crystallographic
41 ordering in the cold-water coral *Lophelia*
42 *pertusa*, *Scientific Reports* 7(1) (2017) 8987.
43 [76] M.V. Kitahara, S.D. Cairns, J. Stolarski, D.
44 Blair, D.J. Miller, A comprehensive
45 phylogenetic analysis of the Scleractinia
46 (Cnidaria, Anthozoa) based on mitochondrial
47 CO1 sequence data, *PLoS One* 5(7) (2010)
48 e11490.
49 [77] A. Meibom, J.-P. Cuif, F. Hillion, B.R.
50 Constantz, A. Juillet-Leclerc, Y. Dauphin, T.
51 Watanabe, R.B. Dunbar, Distribution of
52 magnesium in coral skeleton, *Geophys Res Lett*
53 31(23) (2004).
54 [78] J. Raddatz, V. Liebetrau, A. Rüggeberg, E.
55 Hathorne, A. Krabbenhöft, A. Eisenhauer, F.
56 Böhm, H. Vollstaedt, J. Fietzke, M. López
57 Correa, A. Freiwald, W.C. Dullo, Stable Sr-
58 isotope, Sr/Ca, Mg/Ca, Li/Ca and Mg/Li ratios
59 in the scleractinian cold-water coral *Lophelia*
60 *pertusa*, *Chem Geol* 352 (2013) 143-152.
61 [79] C. Rollion-Bard, D. Blamart, Possible
62 controls on Li, Na, and Mg incorporation into
63 aragonite coral skeletons, *Chem Geol* 396
64 (2015) 98-111.
65 [80] A.A. Finch, N. Allison, Mg structural state
in coral aragonite and implications for the
paleoenvironmental proxy, *Geophys Res Lett*
35(8) (2008).
[81] J.F. Adkins, E.A. Boyle, W.B. Curry, A.
Lutringer, Stable isotopes in deep-sea corals and
a new mechanism for "vital effects", *Geochim*
Cosmochim Acta 67(6) (2003) 1129-1143.
[82] B. Pokroy, J.P. Quintana, E.N. Caspi, A.
Berner, E. Zolotoyabko, Anisotropic lattice
distortions in biogenic aragonite, *Nat Mater*
3(12) (2004) 900-902.
[83] E.H. Gladfeiter, Skeletal development in
Acropora cervicornis: I. Patterns of calcium
carbonate accretion in the axial corallite, *Coral*
Reefs 1(1) (1982) 45-51.
[84] M.D.A.A. Le Tissier, Diurnal patterns of
skeleton formation in *Pocillopora damicornis*
(Linnaeus), *Coral Reefs* 7(2) (1988) 81-88.
[85] M. Gilis, A. Meibom, I. Domart-Coulon, O.
Grauby, J. Stolarski, A. Baronnet,
Biomineralization in newly settled recruits of the
scleractinian coral *Pocillopora damicornis*, *J*
Morphol 275(12) (2014) 1349-65.
[86] M. Hedaka, Fusiform and needle-shaped
crystals found on the skeleton of a coral,
Galaxea fascicularis, Springer Japan, Tokyo,
1991, pp. 139-143.
[87] P.L. Clode, A.T. Marshall, Skeletal
microstructure of *Galaxea fascicularis* exsert
septa: a high-resolution SEM study, *Biol Bull*
204(2) (2003) 146-154.
[88] M. Raz-Bahat, J. Erez, B. Rinkevich, In
vivo light-microscopic documentation for
primary calcification processes in the
hermatypic coral *Stylophora pistillata*, *Cell*
Tissue Res 325(2) (2006) 361-368.
[89] J. Cuif, Y. Dauphin, A. Denis, P. Gautret,
F. Marin, The organo-mineral structure of coral

1
2
3
4 skeletons: a potential source of new criteria for
5 Scleractinian taxonomy, Bull Inst Oceanogr
6 Monaco-Numero Special- (1996) 359-368.

7 [90] J. Stolarski, F.R. Bosellini, C.C. Wallace,
8 A.M. Gothmann, M. Mazur, I. Domart-Coulon,
9 E. Gutner-Hoch, R.D. Neuser, O. Levy, A.
10 Shemesh, A. Meibom, A unique coral
11 biomineralization pattern has resisted 40 million
12 years of major ocean chemistry change, Sci Rep
13 6 (2016) 27579.

14 [91] J. McHale, A. Auroux, A. Perrotta, A.
15 Navrotsky, Surface energies and thermodynamic
16 phase stability in nanocrystalline aluminas,
17 Science 277(5327) (1997) 788-791.

18 [92] L. Yang, C.E. Killian, M. Kunz, N. Tamura,
19 P.U.P.A. Gilbert, Biomineral nanoparticles are
20 space-filling, RSC-Nanoscale 3 (2011) 603-609.

21 [93] F. Podmaniczky, G.I. Tóth, G. Tegze, L.
22 Gránásy, Hydrodynamic theory of freezing:
23 nucleation and polycrystalline growth, Phys Rev
24 E 95(5) (2017).

25 [94] T. Mass, A.J. Giuffre, C.-Y. Sun, C.A.
26 Stiffler, M.J. Frazier, M. Neder, N. Tamura, C.V.
27 Stan, M.A. Marcus, P.U.P.A. Gilbert,
28 Amorphous calcium carbonate particles form
29 coral skeletons, Procs Natl Acad Sci 114(37)
30 (2017) E7670-E7678.

31 [95] Y. Jiang, H. Gong, M. Grzywa, D.
32 Volkmer, L. Gower, H. Cölfen, Microdomain
33 transformations in mosaic mesocrystal thin
34 films, Adv Funct Mater 23(12) (2013) 1547-
35 1555.

36 [96] D.S. Sevilgen, A.A. Venn, M.Y. Hu, E.
37 Tambutté, D. de Beer, V. Planas-Bielsa, S.
38 Tambutté, Full in vivo characterization of
39 carbonate chemistry at the site of calcification in
40 corals, Sci Adv 5(1) (2019) eaau7447.

41 [97] P.W. Voorhees, The theory of Ostwald
42 ripening, J Stat Phys 38(1-2) (1985) 231-252.

43 [98] L. Ratke, P.W. Voorhees, Growth and
44 coarsening: Ostwald ripening in material
45 processing, Springer Science & Business
46 Media2013.

47 [99] C. Stoldt, C.J. Jenks, P.A. Thiel, A.
48 Cadilhe, J.W. Evans, Smoluchowski ripening of
49 Ag islands on Ag (100), J Chem Phys 111(11)
50 (1999) 5157-5166.

51 [100] T. Gerber, J. Knudsen, P.J. Feibelman, E.
52 Granas, P. Stratmann, K. Schulte, J.N.
53 Andersen, T. Michely, CO-induced

Smoluchowski ripening of Pt cluster arrays on
the graphene/Ir (111) moiré, ACS Nano 7(3)
(2013) 2020-2031.

[101] B. Bayerlein, P. Zaslansky, Y. Dauphin,
A. Rack, P. Fratzl, I. Zlotnikov, Self-similar
mesostructure evolution of the growing mollusc
shell reminiscent of thermodynamically driven
grain growth, Nat Mater 13(12) (2014) 1102-7.

[102] R.E. Reed-Hill, R. Abbaschian, Physical
metallurgy principles, 3rd ed., PWS-Kent,
Boston, MA, 1992.

[103] V. Schoeppler, L. Gránásy, E. Reich, N.
Poulsen, R. de Kloe, P. Cook, A. Rack, T.
Pusztai, I. Zlotnikov, Biomineralization as a
paradigm of directional solidification: a physical
model for molluscan shell ultrastructural
morphogenesis, Adv Mater (2018) e1803855.

[104] V. Schoeppler, R. Lemanis, E. Reich, T.
Pusztai, L. Gránásy, I. Zlotnikov, Crystal growth
kinetics as an architectural constraint on the
evolution of molluscan shells, Procs Natl Acad
Sci 116(41) (2019) 20388-20397.

[105] L. Granasy, T. Pusztai, G. Tegze, J.A.
Warren, J.F. Douglas, Growth and form of
spherulites, Phys Rev E 72(1) (2005) 011605.

[106] S. Puvarel, E. Tambutte, L. Pereira-
Mouries, D. Zoccola, D. Allemand, S. Tambutte,
Soluble organic matrix of two Scleractinian
corals: partial and comparative analysis, Comp
Biochem Physiol B Biochem Mol Biol 141(4)
(2005) 480-7.

[107] M.M. Ogilvie, Microscopic and
Systematic Study of Madreporarian Types of
Corals, Phil Trans R Soc London. Series B,
Containing Papers of a Biological Character 187
(1896) 83-345.

[108] R.A. Metzler, D. Zhou, M. Abrecht, J.-W.
Chiou, J. Guo, D. Ariosa, S.N. Coppersmith,
P.U.P.A. Gilbert, Polarization-dependent
imaging contrast in abalone shells, Phys Rev B
77 (2008) 064110-1/9.

[109] I.C. Olson, R.A. Metzler, N. Tamura, M.
Kunz, C.E. Killian, P.U.P.A. Gilbert, Crystal
lattice tilting in prismatic calcite, J Struct Biol
183 (2013) 180-190.

[110] C. Zhong, C.C. Chu, On the origin of
amorphous cores in biomimetic CaCO₃
spherulites: new insights into spherulitic
crystallization, Cryst Growth Des 10(12) (2010)
5043-5049.

1
2
3
4 [111] A. Keller, The spherulitic structure of
5 crystalline polymers. Part II. The problem of
6 molecular orientation in polymer spherulites, J
7 Polym Sci 17(85) (1955) 351-364.
8 [112] E. Ergoz, J. Fatou, L. Mandelkern,
9 Molecular weight dependence of the
10 crystallization kinetics of linear polyethylene. I.
11 Experimental results, Macromol 5(2) (1972)
12 147-157.
13 [113] L. Mandelkern, The relation between
14 structure and properties of crystalline polymers,
15 Polym J 17(1) (1985) 337-350.
16 [114] M. Jenkins, K. Harrison, The effect of
17 molecular weight on the crystallization kinetics
18 of polycaprolactone, Polym Adv Technol 17(6)
19 (2006) 474-478.
20 [115] G. Strobl, W. Hagedorn, Raman
21 spectroscopic method for determining the
22 crystallinity of polyethylene, J Polym Sci:
23 Polym Phys Ed 16(7) (1978) 1181-1193.
24 [116] M. Glotin, L. Mandelkern, A Raman
25 spectroscopic study of the morphological
26 structure of the polyethylenes, Coll Polym Sci
27 260(2) (1982) 182-192.
28 [117] L.S. Taylor, G. Zografi, The quantitative
29 analysis of crystallinity using FT-Raman
30 spectroscopy, Pharm Res 15(5) (1998) 755-761.
31 [118] Y. Yang, M. Chen, H. Li, H. Li, The
32 degree of crystallinity exhibiting a spatial
33 distribution in polymer films, Eur Polym J 107
34 (2018) 303-307.
35 [119] A.G. Shtukenberg, C.T. Hu, Q. Zhu, M.U.
36 Schmidt, W. Xu, M. Tan, B. Kahr, The third
37 ambient aspirin polymorph, Crystal Growth &
38 Design 17(6) (2017) 3562-3566.
39 [120] X. Cui, A.L. Rohl, A. Shtukenberg, B.
40 Kahr, Twisted aspirin crystals, Journal of the
41 American Chemical Society 135(9) (2013)
42 3395-3398.
43 [121] B.A. Palmer, V.J. Yallapragada, N.
44 Schiffmann, E.M. Wormser, N. Elad, E.D.
45 Aflalo, A. Sagi, S. Weiner, L. Addadi, D. Oron,
46 A highly reflective biogenic photonic material
47 from core-shell birefringent nanoparticles,
48 Nature Nanotechnology (2020) 1-7.
49 [122] V.J. Yallapragada, D. Oron, Optical
50 properties of spherulite opals, Optics letters
51 44(23) (2019) 5860-5863.
52 [123] B. Miao, D.N. Wood, W. Bian, K. Fang,
53 M.H. Fan, Structure and growth of platelets in

graphite spherulites in cast iron, Journal of
materials science 29(1) (1994) 255-261.

[124] V.A. Fernandes, A.J. Müller, A.J.
Sandoval, Thermal, structural and rheological
characteristics of dark chocolate with different
compositions, Journal of Food Engineering
116(1) (2013) 97-108.

Table 1. Summary of all coral species studied here, and the crystal structures observed in their mature skeletons.

Table 2. Specific surface area data measured by Brunauer-Emmett-Teller (BET) method Coral skeletons measured here by the are as space-filling as single crystals of geologic aragonite. The BET results are typical of biogenic minerals, similar to those previously published for sea urchin spines, spicules, and teeth [1], and very different from those usually measured for aggregates of nanoparticles, which are typically in the 200-300 m²/g range and thus highly porous [2].

Figure 1. Scanning electron microscopy (SEM) images of corallites from three distantly related coral genera: *Balanophyllia*, *Porites*, and *Cyphastrea* (top row). The bulk mature skeleton is always spherulitic (middle row), but the fine-scale morphology at the growth front varies widely across corals (bottom row).

Figure 2. Merged PIC maps of (a) *Stylophora pistillata* (*Sp*) and (b) *Balanophyllia europaea* (*Be*) coral skeletons. (c) Color bar for PIC maps in (a) and (b). Centers of calcification (CoC) extend along a non-straight line between the two CoC labels in *Sp*. No CoCs are visible in this particular *Be* region. Notice the acicular crystal fibers (F) characteristic of spherulites, changing color and thus orientation only slightly across grain boundaries, and sprinkles (S), which are smaller crystals changing color abruptly across boundaries. Sprinkles are found in the mature (bulk) skeletons of *Be*, but not in *Sp*, whereas spherulitic crystals appear in both skeletons. Inset in (b) shows a higher magnification PIC map of the sprinkles, which are indicated by the arrows and are interspersed with spherulitic crystals. (d) Distributions of angular distances between the *c*-axes of adjacent crystals in spherulitic crystals in *Sp* and *Be* skeletons, and in concentric rings of *Acropora pharaonis* (*Ap*) skeletons (Fig. 7). (e) Identically measured distributions in the sprinkles of *Be*, *Oculina patagonica* (*Op*), and *Ap* skeletons. Notice that in spherulitic crystals, the angular distances are always within 35°, whereas in sprinkles, they are random (0–90°). Details of the angular distance measurement and the ROI selections are described in the Experimental Methods and Figure S4.

Figure 3. PIC maps of the 5 coral species that exhibit abundant small (0.2-2µm) sprinkles across their skeletons. These are *Phyllangia americana mouchezii* (*Pam*), *Oculina patagonica* (*Op*), *Acropora pharaonis* (*Ap*), *Balanophyllia europaea* (*Be*), and *Blastomussa merleti* (*Bm*). Sprinkles (S) appear as randomly colored and oriented crystals smaller than fiber (F) crystals. In *Ap* they are localized in centers of calcification (CoCs, between pairs of CoC labels), in *Op* and *Be* at the surfaces of fiber bundles, which during coral skeleton growth were the growth fronts (GF, between pairs of GF labels). In *Pam* and *Bm* sprinkles appear everywhere interspersed with fibers. The box in d is magnified in Figure 6d.

Figure 4. PIC maps of the 4 coral species that exhibit large (2-20µm) sprinkles across their skeletons. These are *Blastomussa merleti* (*Bm*), *Madracis pharensis* (*Mp*), *Favia* sp. (*Fs*), and - *Balanophyllia europaea* (*Be*). Arrows indicate a few large sprinkles, but many more are visible. Large sprinkles are distinct from fibers (F) not by size but by crystal orientations: they form >35° angles with their neighboring crystals, whereas fiber crystals only form small angles (<35°) with respect adjacent fibers in the same bundle. Nanoparticulate crystals (between pairs of CoC labels) are visible in the CoCs of *Mp* and *Be*. Nanocrystals in the CoCs are not randomly oriented, but rather oriented similarly to their neighboring crystals. CoCs, therefore, cannot be sprinkles.

Figure 5. PIC maps of the 5 coral species that exhibit few or no sprinkles. These are *Turbinaria peltata* (*Tp*), *Stylophora pistillata* (*Sp*), *Porites lutea* (*Pl*), *Montipora turgescens* (*Mt*), and *Micromussa lordhowensis* (*Ml*). Again centers of calcification (CoCs, between pairs of CoC

labels) are distinguishable by their nanoparticulate appearance along a straight line in Tp , a long tortuous line in Sp , four parallel lines in Pl only one of which is between CoC labels, and in Mt . As in **Figure 4**, none of these CoCs exhibit any sprinkles. Arrows indicate the very few visible sprinkles. These are so few that they could belong to out-of-plane bundles of fibers, thus these 5 species are described as non-sprinkle retaining.

Figure 6. a: PIC map of *Acropora pharaonis* (Ap) coral skeleton, showing sprinkles (S) concentrated at the CoCs (between pairs of CoC labels), spherulitic crystal fibers (F) fanning out from the CoCs, and concentric rings (R), which consist of finer spherulitic fiber crystals. Boxes b, c indicate the areas magnified in panels b, c. **b:** Magnified concentric rings, showing that these are made of nearly co-oriented acicular crystals. **c:** Magnified sprinkles from CoCs. **d:** Sprinkles at the boundary of CoCs and fiber crystals, magnified from the box area in **Figure 3d**. Arrows indicate two blue sprinkles that expand radially into -30° oriented fibers. Red and green sprinkles do not grow as they run into other crystals. In panels a and d pixels are 60 nm, in b and c they are 20 nm.

Figure 7. Schematic of spherulite growth mechanisms. All cases **a, b, c** share growth front nucleation (GFN), and, in the final spherulite, radial crystals oriented and thus colored similarly to their neighboring crystals. **a.** This is the spherulite formation mechanism proposed here: All newly nucleating crystals have random orientations (small hexagons with diverse colors, termed sprinkles), and because of competition for space they grow only if they are radially oriented. Coarsening makes larger crystals grow at the expense of smaller crystals, thus resulting in sprinkle-free spherulites. **b.** In a subset of coral skeletons the sprinkles are retained, because of incomplete or absent coarsening. These are the exceptional cases suggesting the formation mechanism for all spherulites, potentially. **c.** All newly nucleating crystals have orientation similar but not identical to the mother crystal. This previous assumption was termed non-crystallographic branching, and is ruled out by the alternative growth mechanism in **a**, inspired by coral skeletons.

Figure 8. Phase-field simulation of spherulitic growth from sprinkles. **a-d:** Time series of the spherulite growth from sprinkles, showing frames 6, 21, 41, 60 of the simulation. **a:** An early frame in which sprinkles are formed, with random orientation, by nucleation from a solution with high supersaturation. **b,c,d:** Elongated crystal fibers grow from each sprinkle. Radially oriented crystals continue to elongate, whereas transversally oriented ones abut one another and stop growing. This growth process ultimately results in radially oriented crystals with slight misorientation across grain boundaries, that is, spherulitic growth. Notice that sprinkles nucleate at the liquid-solid interface during GFN. Three white boxes and three black boxes are positioned in identical locations in b, c, d, and are centered around a sprinkle that persists or disappears, respectively. **e:** Magnified images of the details boxed in b,c,d, panels shown as a function of time in each b,c,d triplet. At the center of the white boxes the sprinkle persists while other sprinkles disappear. In the black boxes at the bottom, almost all sprinkles disappear due to coarsening, which may occur by Ostwald or Smoluchowski ripening, if the system is locally liquid or solid, respectively. Locally slow, incomplete, or gradual solidification enables sprinkle shrinking or rotation.

Figure 9. Phase-field simulation of coral skeleton grown from sprinkles. **a:** Simulated orientation map in which sprinkles form at the tip of each branch, termed nubbin, and become the core of each branch, where they persist. Much larger crystals form on the branch sides, which are similar to the large sprinkles (2-20 μm). **b,c:** PLM images from two distinct *Acropora pharaonis* (Ap) coral skeletons. The top two panels in b are cropped and magnified from the areas indicated by magenta boxes in c, the bottom two panels are from a different Ap skeleton. The

overall morphology in c, and the details in b, including sprinkles at the center, and fibers at the sides of each nubbin, are all similar to the simulated ones in a, except that the fibers in b and c are elongated and thinner than the side crystals in a.

[1] L. Yang, C.E. Killian, M. Kunz, N. Tamura, P.U.P.A. Gilbert, Biomineral nanoparticles are space-filling, *RSC-Nanoscale* 3 (2011) 603-609.

[2] J. McHale, A. Auroux, A. Perrotta, A. Navrotsky, Surface energies and thermodynamic phase stability in nanocrystalline aluminas, *Science* 277(5327) (1997) 788-791.

Figure 1
[Click here to download high resolution image](#)

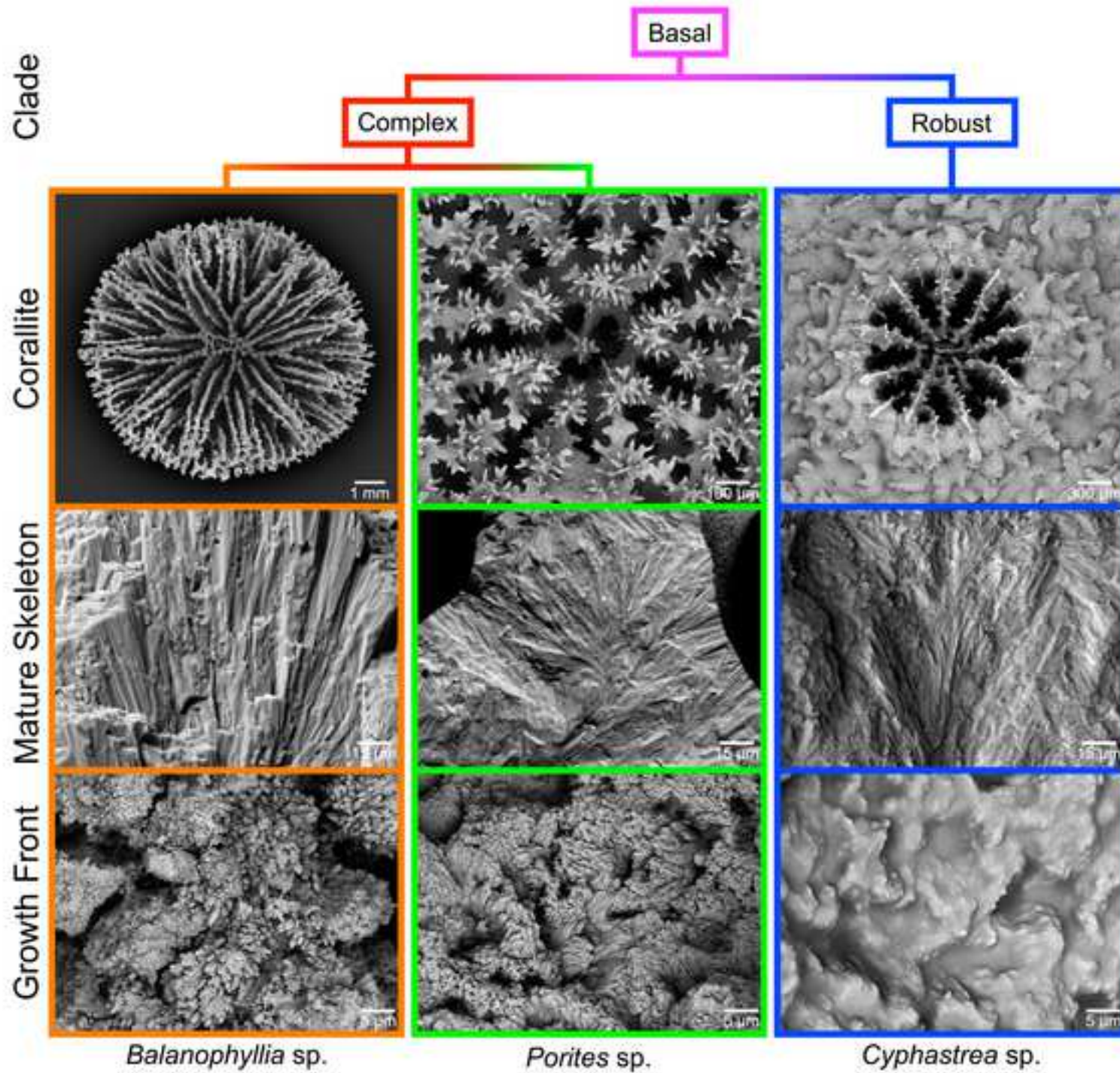


Figure 2
[Click here to download high resolution image](#)

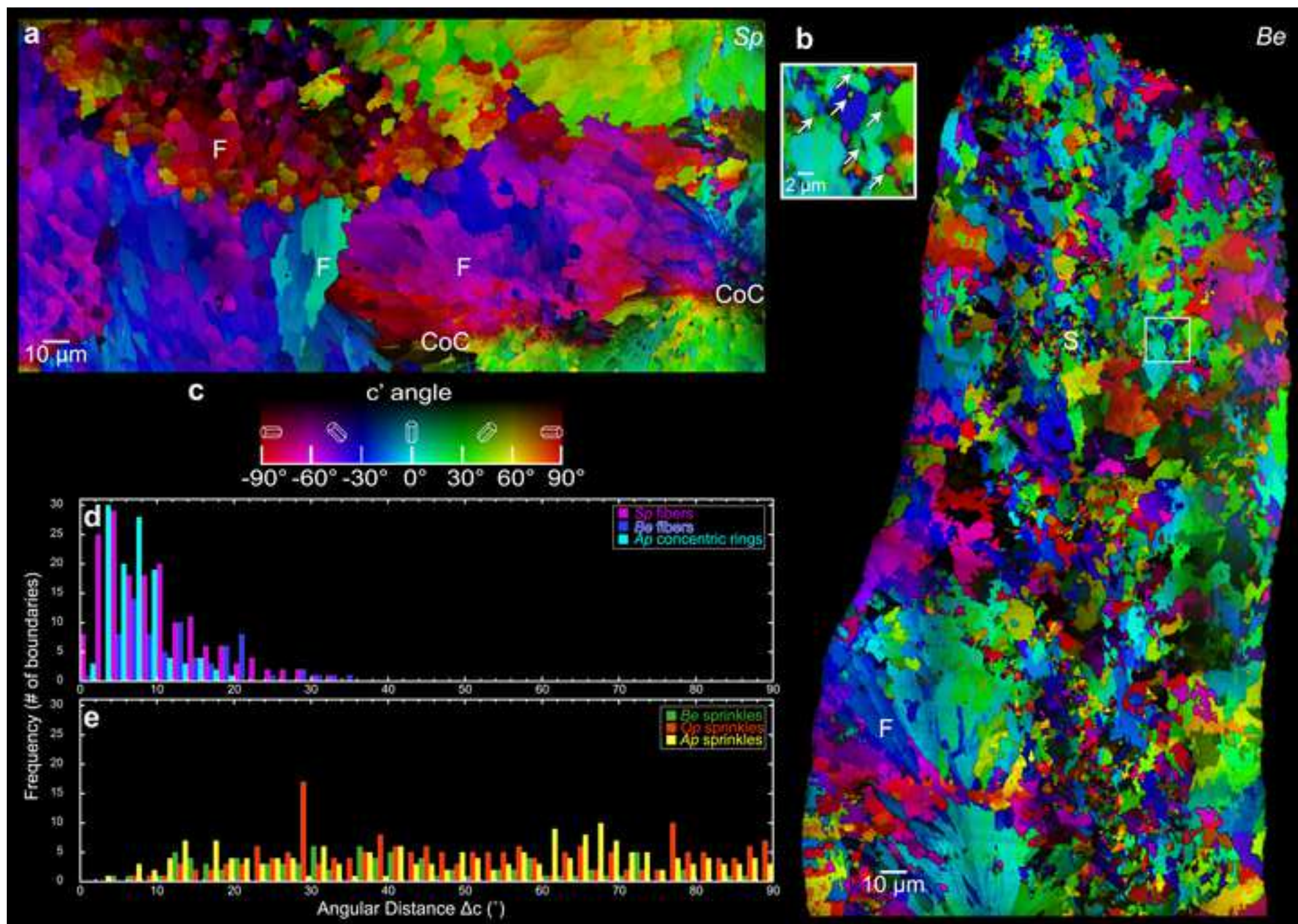


Figure 3
[Click here to download high resolution image](#)

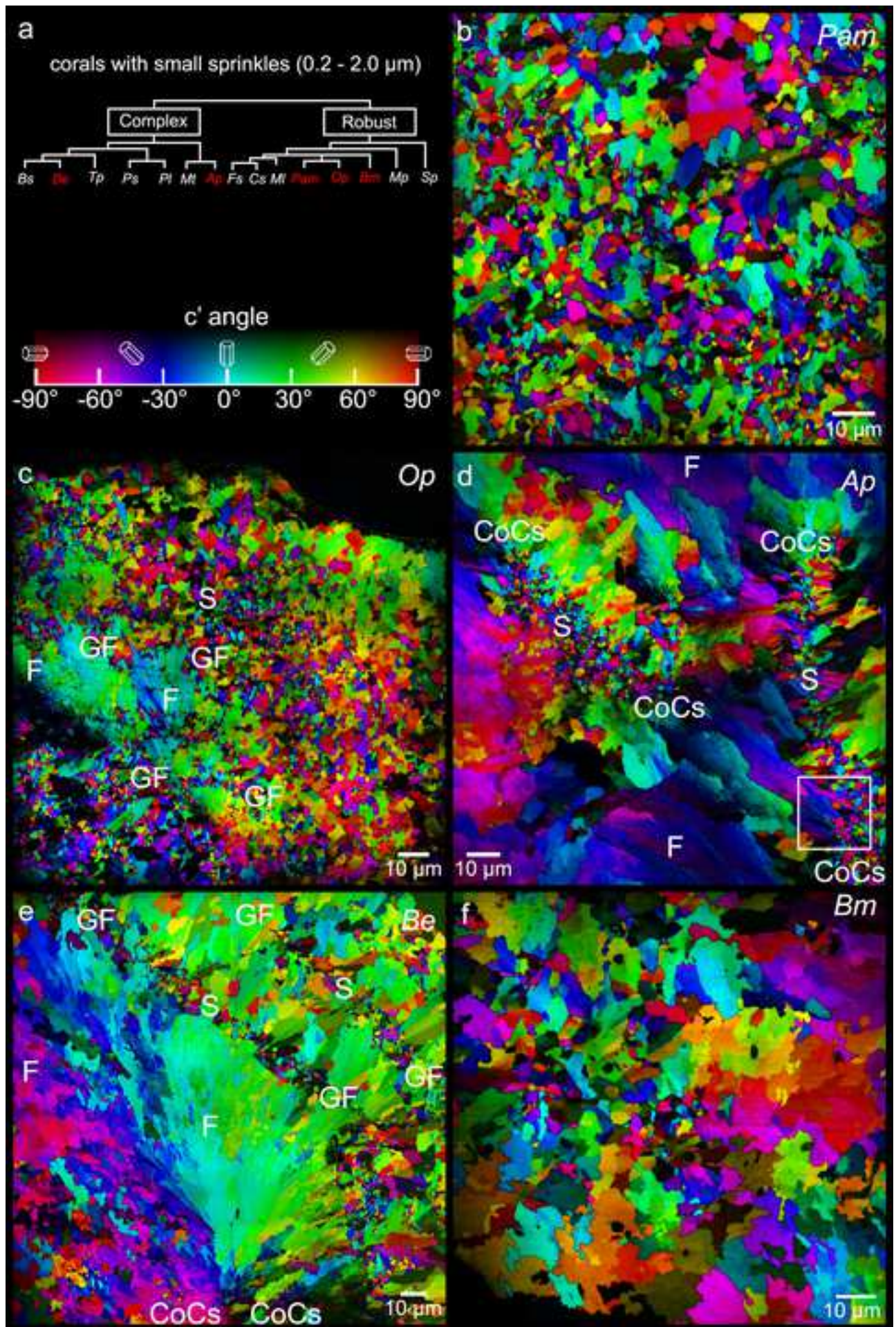


Figure 4
[Click here to download high resolution image](#)

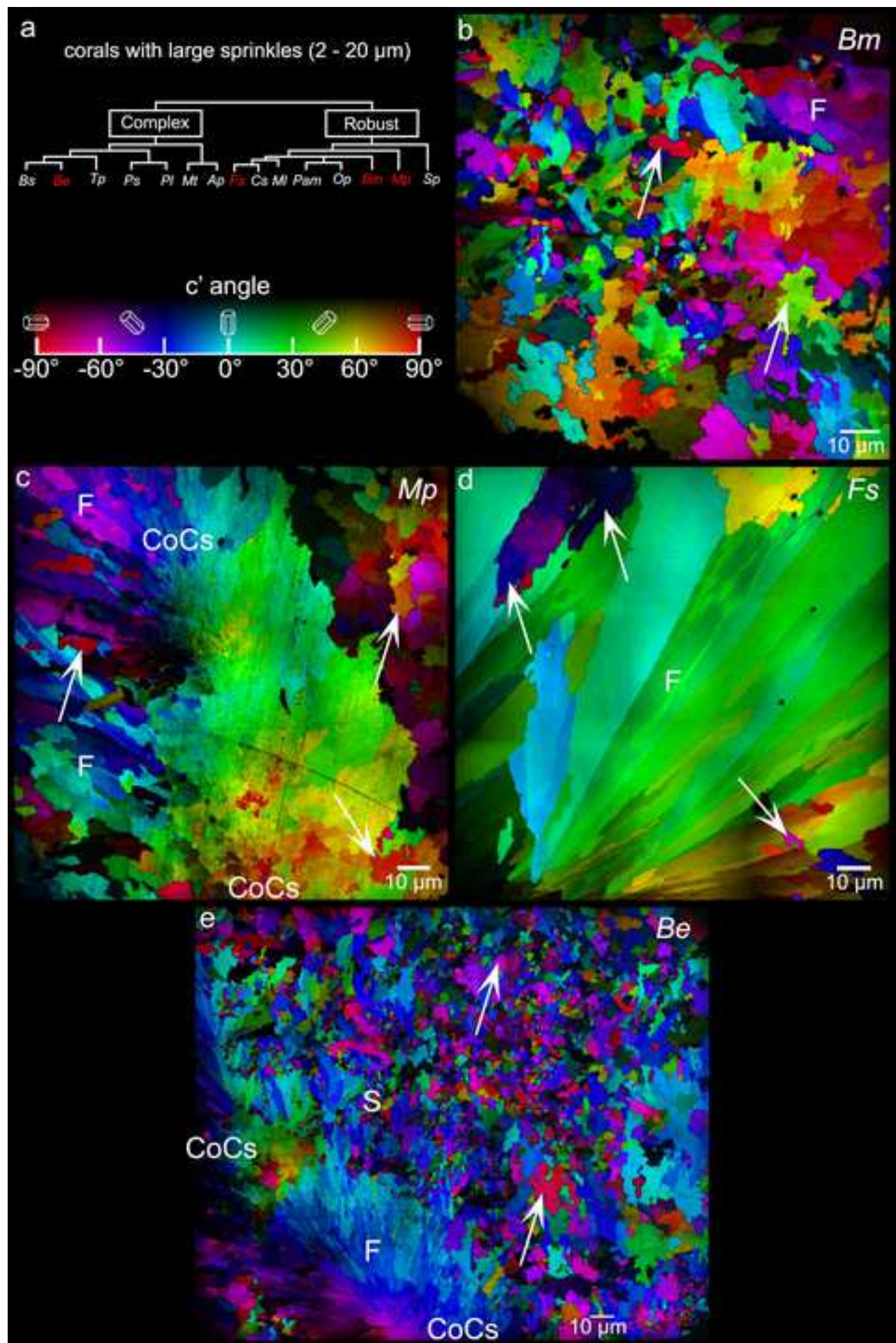


Figure 5
[Click here to download high resolution image](#)

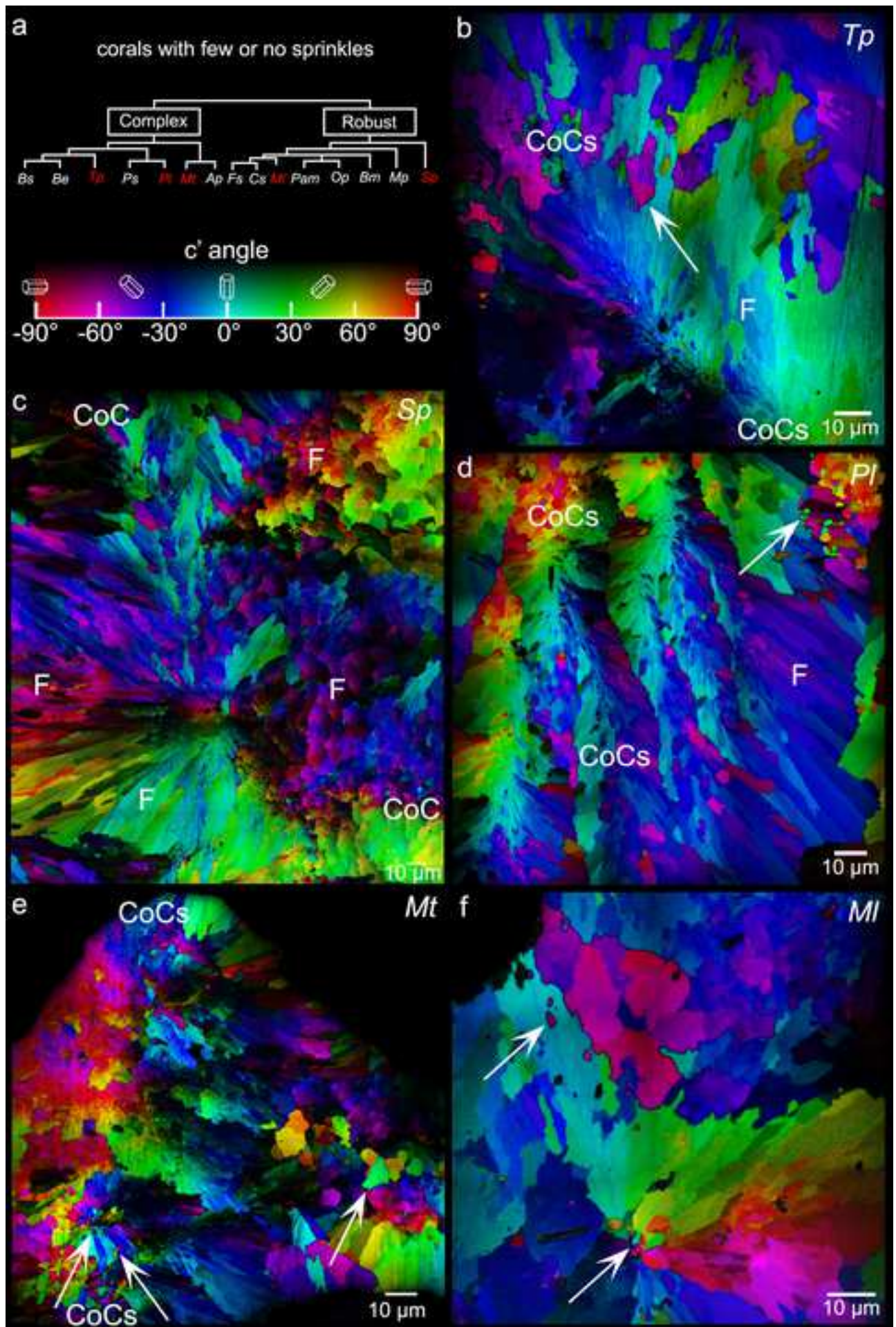


Figure 6
[Click here to download high resolution image](#)

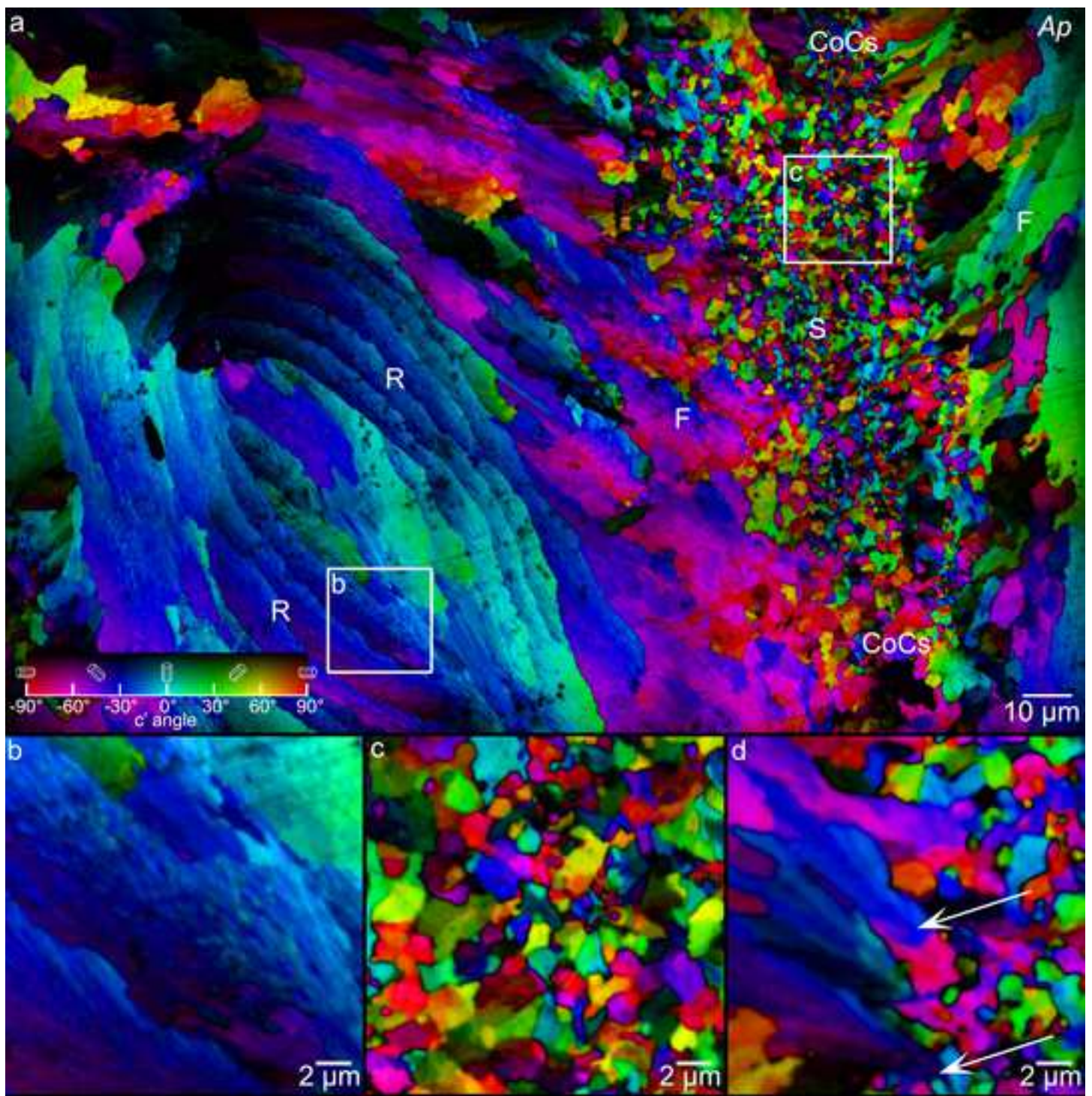


Figure 8
[Click here to download high resolution image](#)

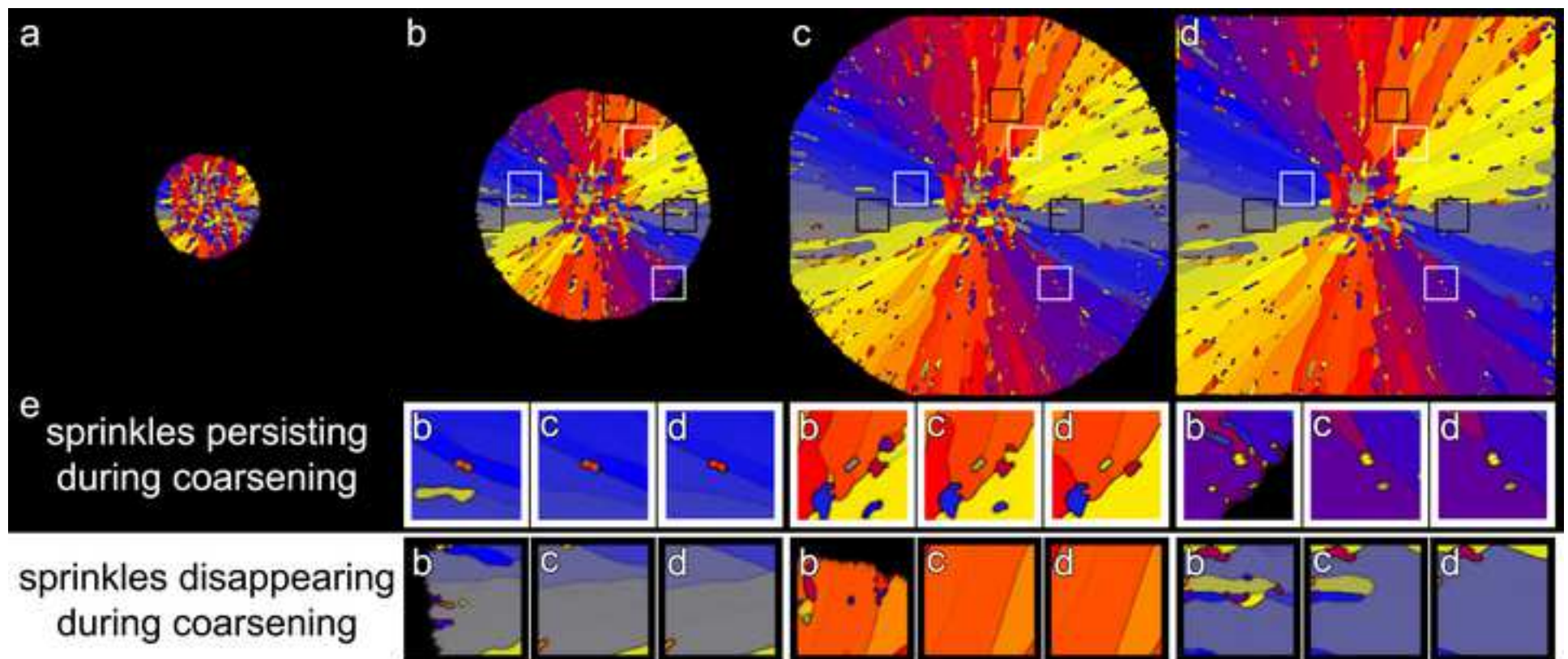


Figure 9
[Click here to download high resolution image](#)

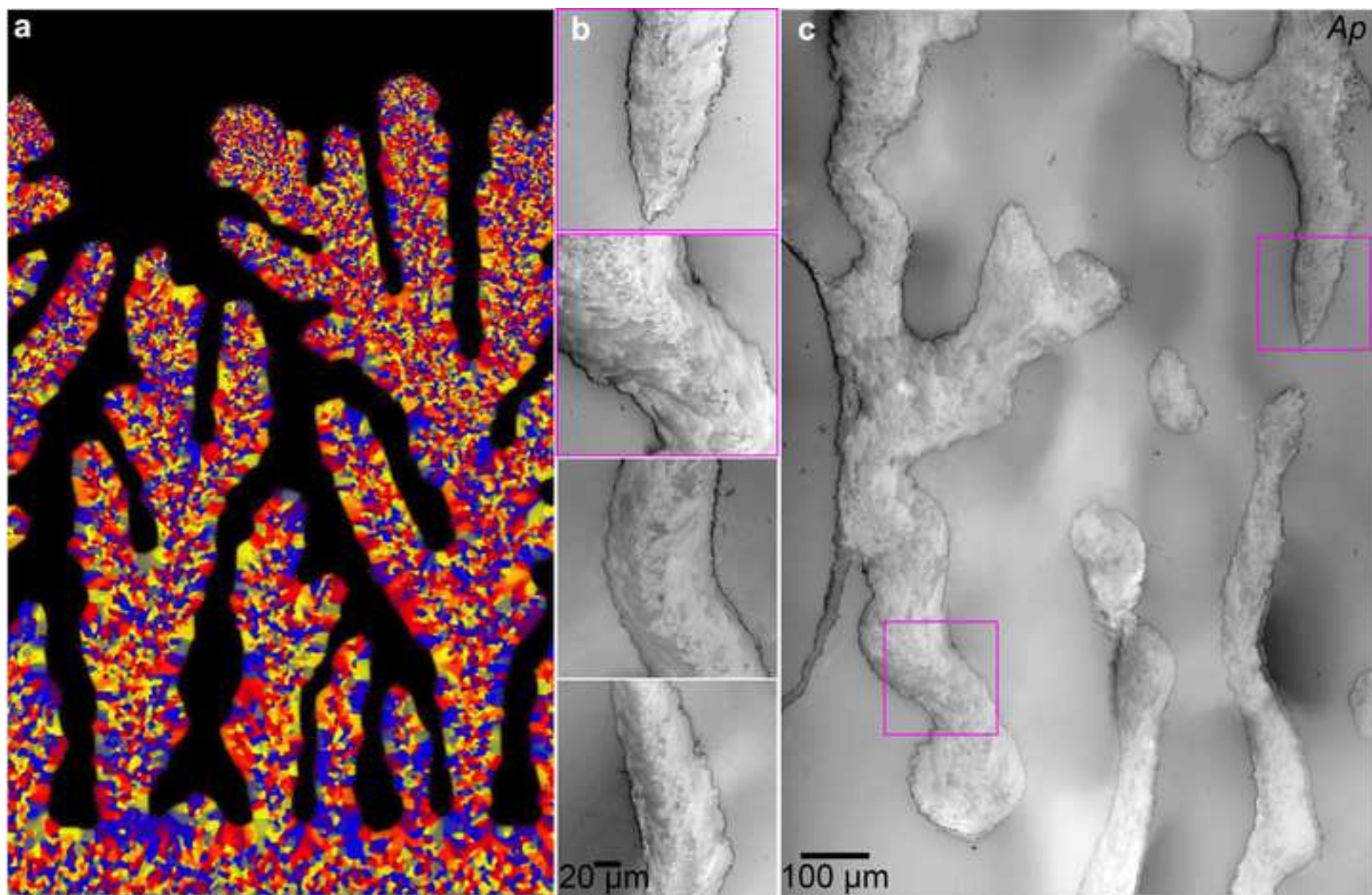


Figure 7
[Click here to download high resolution image](#)

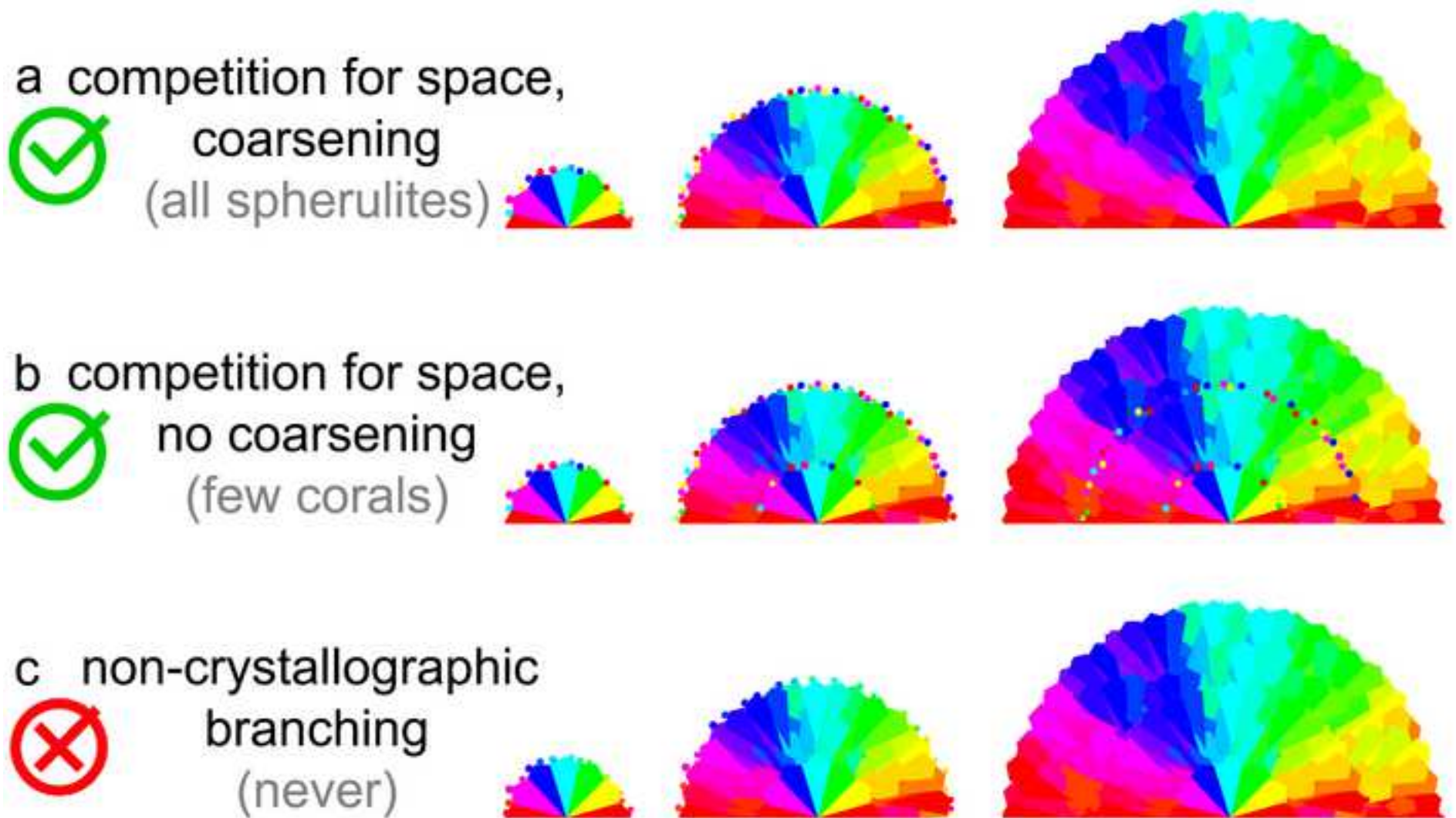


Table 1

Table 1. Summary of all coral species studied here, and the crystal structures observed in their mature skeletons.

Coral skeleton structures observed			Genus and species	Clade	Morphology	Geographic origin	Climate
spherulitic fibers and CoCs	small sprinkles (0.2-2 μm)		<i>Stylophora pistillata</i> (Sp)	Robust	Branching	Red Sea	sub-tropical
			<i>Turbinaria peltata</i> (Tp)	Complex	Table-like	Indo-Pacific	tropical
			<i>Porites lutea</i> (Pl)	Complex	Massive	Red Sea	sub-tropical
			<i>Montipora turgescens</i> (Mt)	Complex	Encrusting	Indo-Pacific	tropical
			<i>Micromussa lordhowensis</i> (Ml)	Robust	Massive	Indo-Pacific	tropical
			<i>Phyllangia americana mouchezii</i> (Pam)	Robust	Encrusting	Mediterranean Sea	temperate
	large sprinkles (2-20 μm)	concentric rings	<i>Oculina patagonica</i> (Op)	Robust	Encrusting	Mediterranean Sea	temperate
			<i>Acropora pharaonis</i> (Ap)	Complex	Branching	Red Sea	sub-tropical
			<i>Blastomussa merleti</i> (Bm)	Robust	Massive	Indo-Pacific	tropical
			<i>Balanophyllia europaea</i> (Be)	Complex	Solitary	Mediterranean Sea	temperate
			<i>Madracis pharensis</i> (Mp)	Robust	Encrusting	Mediterranean Sea	temperate
			<i>Favia</i> sp. (Fs)	Robust	Massive	Red Sea	sub-tropical

Table 2. Specific surface area data measure by Brunauer-Emmett-Teller (BET) method Coral skeletons measured here by the are as space-filling as single crystals of geologic aragonite. The BET results are typical of biogenic minerals, similar to those previously published for sea urchin spines, spicules, and teeth [1], and very different from those usually measured for aggregates of nanoparticles, which are typically in the 200-300 m²/g range and thus highly porous [2].

sample ID	specific surface area (m ² /g) 1 st measurement	specific surface area (m ² /g) 2 nd measurement	average
<i>Sp</i> coral skeleton	3.78	3.53	3.53±0.18
<i>Be</i> coral skeleton	4.64	3.91	4.28±0.52
Geologic aragonite	1.67	1.73	1.70±0.04

[1] L. Yang, C.E. Killian, M. Kunz, N. Tamura, P.U.P.A. Gilbert, Biomineral nanoparticles are space-filling, *RSC-Nanoscale* 3 (2011) 603-609.

[2] J. McHale, A. Auroux, A. Perrotta, A. Navrotsky, Surface energies and thermodynamic phase stability in nanocrystalline aluminas, *Science* 277(5327) (1997) 788-791.

Supplementary Material

[Click here to download Supplementary Material: AB-20-1031 \(Appendix A-9PG\)-without highlighting.docx](#)

Supplementary Material

[Click here to download Supplementary Material: AB-20-1031 \(Appendix B-3PG\)-without highlighting.docx](#)